The Nrd1p-Nab3p-Sen1p complex constitutes a vital component of the nuclear mRNA surveillance in *Saccharomyces cerevisiae*

Pragyan Singh, Neeraja Marathe & Biswadip Das*

Department of Life Science and Biotechnology, Jadavpur University, Kolkata, India.

*Correspondence:
Dr. Biswadip Das
Department of Life Science and Biotechnology
Jadavpur University
188 Raja S.C. Mullick Road
Kolkata – 700 032
West Bengal
India
Phone: 91-9748324755 (Cell)
E. mail: biswdip.das@jadavpuruniversity.in, biswadipdas22@gmail.com

Character Count: 26,983 (without spaces)

Keywords
CTEXT/mRNA degradation/ Nuclear Exosome/NNS Complex/TRAMP

Running title: NNS Complex is a Fundamental Decay Factor
Abbreviations: TRAMP, **TR**f4-**A**ir1/2-**M**tr4 **P**olyadenylation; CTEXT, **C**bc1-**T**if4631-dependent **EX**osomal **T**argeting; NNS, **N**rd1p-**N**ab3p-**S**en1p.

EMBOR-2020-51007V1_Manuscript.docx (Abstract + Text + Acknowledgement + References + Tables 1-4 + Legends to Figures1-5 + Tables EV1-3 + Legends to Figures EV1-5)
Tables 1-4
Fig. 1 (EMBOR-2020-51007V1_Fig1.eps)
Fig. 2 (EMBOR-2020-51007V1_Fig2.eps)
Fig. 3 (EMBOR-2020-51007V1_Fig3.eps)
Fig. 4 (EMBOR-2020-51007V1_Fig4.eps)
Fig. 5 (EMBOR-2020-51007V1_Fig5.eps)
Extended View Figures EMBOR-2020-51007V1 EV1-5.pdf
EMBOR-2020-51007V1_Source Data_Figure1-5
EMBOR-2020-51007V1_Source Data_Figure1-5

Abstract (Required 175 words, Actual 159 words)

In *Saccharomyces cerevisiae*, the NNS (Nrd1p-Nab3p-Sen1p) complex along with the nuclear exosome, TRAMP, and CTEXT rapidly degrades aberrant mRNAs. Consistently, *nrd1-1/nrd1-2* mutant cells displayed an impairment of the decay of all kinds of aberrant mRNAs, just like the yeast mutants deficient in Rrp41p, Rrp6p, and Rrp4p. Interestingly, however, *nrd1*Δ^{CID} mutant strain (in which Nrd1p failed to interact with RNAPII) exhibits a selective abrogation of the degradation of aberrant messages generated during transcription elongation, splicing and 3′-end maturation, without affecting the decay rate of the export-defective mRNAs. Mutation in the 3′-end processing factor, Pcf11p, in contrast, displayed a selective abolition of the decay of the export-defective mRNAs without influencing the faulty messages spawned in the early phase of mRNP biogenesis. Thus, mRNA decay by Nrd1p is accompanied by its co-transcriptional recruitment onto the faulty messages, which initially relies on RNAPII during transcription elongation and on Pcf11p post-transcription. Furthermore, Nrd1p binding to the export-defective messages leads to the recruitment of Rrp6p to promote their decay.

Introduction

Aberrant messages derived from the inaccurate mRNP biogenesis are eliminated by a broad spectrum of mRNA surveillance and quality control mechanisms (Parker, 2012; Das & Das, 2013; Mitchell, 2014; Kilchert *et al.*, 2016). In *Saccharomyces cerevisiae*, the nuclear exosome, along with its cofactors, degrade a wide array of aberrant and normal mRNAs (Mitchell et al. 1997, Butler, 2002; Parker, 2012; Das & Das, 2013; Allmang *et al.*, 2000). Functionally, these cofactors recognize specific RNA targets and then further recruit them to the core exosome ($EXO11^{Dis3p+Rrp6p}$) to promote their degradation (Schmidt & Butler, 2013). TRAMP (**TR**f4p/5p-**A**ir1p/2p-**M**tr4p-**P**olyadenylation) complex, the best-studied cofactor in *S.* cerevisiae consists of DExH box helicase, Mtr4p (Halbach *et al*, 2013; Hardwick & Luisi, 2013; Kilchert *et al*, 2016), non-canonical poly(A) polymerase, Trf4p/Trf5p and Zn-knuckle RNA binding proteins, Air1p/2p (Halbach *et al*, 2013; Hardwick & Luisi, 2013; Kilchert *et al*, 2016). In addition to TRAMP, another cofactor, CTEXT (**C**bc1p-**T**if4631p-dependent **EX**osomal **T**argeting) (previously termed as DRN) (Maity *et al*, 2016), consisting of nuclear cap-binding protein Cbc1p/2p (Das *et al*, 2000, 2003), shuttling proteins Tif4631p/ Upf3p (Das *et al*, 2014), a DEAD-box RNA helicase, Dbp2p (Cloutier *et al*, 2012) and meiotic protein Red1p (Eichinger & Jentsch, 2010), degrades a distinct group of aberrant mRNAs.

Aberrant mRNAs in the yeast nucleus were classified into early, intermediate, and late depending on the specific phases of mRNP biogenesis events at which they are generated (Table 1). The transcription-elongation and splice-defective messages were classified as early, the aberrant 3′-end processing-defective transcripts were categorized as intermediate, and the export-defective messages were classified as the late category (Maity *et al*, 2016). Remarkably, while the nuclear exosome degrades all of these messages, the TRAMP degrades only the faulty messages derived in the early phase, and the CTEXT degrades only the faulty transcripts produced during the terminal stage of

mRNP biogenesis (Maity *et al*., 2016). Strikingly, the degradation of aberrant messages derived at the intermediate stage of mRNP biogenesis requires both TRAMP and CTEXT (Maity *et al*, 2016). However, the molecular basis of the stage-specific participation of TRAMP and CTEXT onto the distinct classes of aberrant messages is still unclear.

The RNA binding protein Nrd1p, complexed with its partners, Nab3p (another RNA binding protein) and Sen1p (a putative helicase), dubbed NNS (Nrd1p-Nab3p-Sen1p) complex, participates in transcription termination of pre-snRNAs, pre-snoRNAs, and Cryptic Unstable Transcripts (CUTs) (Steinmetz *et al*, 2001), thereby leading either to their maturation or degradation by the exosome and TRAMP (Steinmetz & Brow, 1998; Vasiljeva & Buratowski, 2006). This complex also degrades (i) antisense mRNA/transcripts, (ii) bacterial Rho helicase-induced aberrant mRNAs (Honorine *et al*, 2011; Moreau *et al*, 2019), and (iii) a few normal mRNAs (Bresson *et al*, 2017). Notably, the decay of Rho-induced aberrant transcripts involved the Nrd1p-dependent co-ordinated recruitment of Rrp6p after being recruited by the RNAP II (Honorine *et al*, 2011). In an extension of this investigation, genome-wide high-resolution landscapes of Rrp6p, Trf4p, and Nrd1p/Nab3p were utilized to show that Nrd1p/Nab3p redistribute from the genomic loci producing non-coding RNAs to Rho-affected protein-coding genes, thereby triggering their decay and elimination (Moreau *et al*, 2019). Despite this study assigns a functional role of Nrd1p/Nab3p in the quality control of anomalous transcripts lacking mRNA processing factors, the role of Nrd1p complex in the surveillance of entire spectrum of aberrant mRNAs was never addressed. Moreover, the precise relationship of NNS with the nuclear exosome/TRAMP/ CTEXT remained largely unexplored. In this work, we present evidence that Nrd1p (and presumably the NNS complex) plays a central role in the surveillance of entire spectrum of aberrant nuclear mRNAs. Moreover, the co-transcriptional recruitment of Nrd1p (i) on all kinds of faulty transcripts is found to be crucial for their decay and (ii) on the export-defective mRNAs leads to the recruitment of

the exosome component Rrp6p. Our evidence suggests that mode of recruitment of Nrd1p onto a given aberrant message is also vital to govern if it would further facilitate the TRAMP- or CTEXT-dependent degradation of distinct class of faulty messages.

Results and Discussion

We initiated this study with a major pursuit (i) if the NNS complex plays a universal role in the nuclear degradation of the entire spectrum of aberrant messages, and (ii) to unfold the functional relationship of NNS with the TRAMP/CTEXT/ exosome. Using a holistic approach, we analyzed its functional role in the nuclear decay of various kinds of aberrant nuclear messages (Table 1) by comparing their steady-state levels and stability in isogenic series of strains. These series consist of a parent strain defective in a given type of mRNP biogenesis and isogenic derivative of the parent, which additionally harbor various mutations in the *NRD1* gene (see below). This stability analysis was then followed by the systematic investigations of Nrd1p and Rrp6p occupancy onto various kinds of aberrant messages to have an insight into the mechanism of how the Nrd1p recruitment is taking place onto a specific kind of aberrant messages and how the Nrd1p recruitment further influence the downstream fate of the aberrant messages.

Nrd1p participates in the degradation of aberrant mRNAs generated in the early, intermediate and late phases of mRNP biogenesis

During transcription elongation of the protein-coding genes in eukaryotes, a complex of Hpr1p, Tho2p, Mft1, Thp2 (dubbed THO complex) is deposited onto transcribing messages, which leads to its subsequent association with the splicing/export factors Sub2p/Yra1p to promote their mRNP maturation and export (Libri *et al*, 2002; Strasser *et al*, 2002; Zenklusen *et al*, 2002). Mutation in any of the THO components (generating a *hpr1*-Δ or *mft1*-Δ strain) led to the destabilization of several transcripts, (Libri *et al*, 2002; Zenklusen *et al*, 2002; Rougemaille *et al*, 2007), which were rescued by

the inactivation of the nuclear exosome, and TRAMP, but not by the inactivation of CTEXT (Maity *et al*, 2016). Similarly, a mutation in *PRP2* gene (generating a *prp2-1* strain) encoding an essential splicing factor (Plumpton *et al*, 1994) resulted in the accumulation of splice-defective pre-mRNAs in the nucleus at a non-permissive temperature of 37ºC, which were rapidly degraded by the nuclear exosome (Bousquet-Antonelli *et al*, 2000) and TRAMP complex (Kong *et al*, 2014; Maity *et al*, 2016). In the conditionally lethal *rna14-1/rna15-2* strains, defective in 3′-end processing, globally defective transcripts are readily produced at restrictive temperature of 37°C, which harbor aberrantly long 3′-extended read-through termini (Birse *et al*, 1998; Minvielle-Sebastia & Keller, 1999; Proudfoot, 2000; Yonaha & Proudfoot, 2000). These defective transcripts were processed by the nuclear exosome to their natural length (Libri *et al*, 2002; Torchet *et al*, 2002) and consequently were found to be stabilized by the mutations either in the components of the nuclear exosome, TRAMP and CTEXT (Maity *et al*, 2016). These data collectively suggested that assembly- and splice-defective mRNPs in *hpr1*-Δ and *prp2-1* strains (early) undergo degradation in the exosome/ TRAMP-dependent manner. In contrast, the decay of the read-through transcripts in *rna14-1/15-2* strains (intermediate) requires the exosome/TRAMP/CTEXT complex and the export-defective mRNAs (late) messages require the action of the exosome/CTEXT (Table1) (Maity *et al*, 2016).

To assess the role of Nrd1p in the decay of the transcription-elongation-, splice- and 3′-end processing-defective transcripts, we determined the steady-state levels of two arbitrarily chosen model mRNAs produced in each of the three isogenic yeast strain series at a non-permissive temperature of 37°C (Maity *et al*, 2016). These series consist of a parent strain defective in transcription elongation (*hpr1*-Δ), splicing (*prp2-1*), and 3′-end processing (*rna14-1*) events and derivative of this parent with various mutations in *NRD1* gene as indicated in Table EV1 and Fig 1. We used three different mutations in the *NRD1* gene, the first two (*nrd1-1*, and *nrd1*-2) harbor pre-mature non-sense mutations

leading to the formation of two truncated versions of Nrd1p. The last one (*nrd1*Δ^{CID}) carries a deletion of its CID (RNAPII **C**TD **I**nteracting **D**omain) that abolishes the ability of the mutant *nrd1*Δ^{CID} protein to interact with RNAPII (Vasiljeva & Buratowski, 2006; Steinmetz & Brow, 1998). Remarkably, all of the test transcripts (*ACT1*, and *CYC1 in hpr1*-Δ background, pre-*ACT1* and pre-*CYH2* in the *prp2-1* background, and *LYS2* and *CYC1* in the *rna14-1* background) displayed a robust stabilization (varying from three to nine-folds in different mutant strains) in *rrp6*-Δ, *nrd1-1*, *nrd1-2*, and *nrd1*Δ^{CID} strains at the non-permissive temperature of 37°C (Fig 1). Notably, no significant alteration in the steady-state levels of the same test messages in the same isogenic yeast strain series was observed at a permissive temperature of 25°C (Fig EV1). As noted before (Maity *et al*, 2016), none of these aberrant mRNAs did display any stabilization in *hpr1*-Δ and *prp2-1* isogenic background when CTEXT component Cbc1p was deleted but showed a significant stabilization of the two test mRNAs in *rna14-1* strain background (Fig 1). To further corroborate the enhancement of the steady-state levels of these transcripts in various *nrd1* mutant strains, the decay rates of these faulty messages was determined in wild-type and various *nrd1* strain backgrounds, all of which collectively revealed that their decay rates were significantly diminished in *nrd1-1*, *nrd1-2* and *nrd1*Δ^{CID} strains in comparison to that of the corresponding wild type strains (Fig 2A-E, Table 2). Collective data is thus consistent with the conclusion that transcription-elongation/ assembly defective, splice-defective and aberrantly long read-through transcripts with 3′-extensions are subject to the nuclear degradation by Nrd1p.

A variety of nucleus-retained export inefficient messages are generated during the terminal phase of the mRNP biogenesis in the baker's yeast which is classified into three different categories, such as (i) those that are generated due to a *cis*-acting mutation in their transcript body, as exemplified by *lys2-187* mRNA (Das *et al*, 2006), (ii) global poly(A)$^+$ messages retained in the nucleus of temperature-sensitive *nup116*-Δ mutant yeast strain (Das *et al*, 2003) at the restrictive condition of

37°C due to complete block of nuclear export (Wente & Blobel, 1993), and (iii) naturally occurring nucleus-retained export-inefficient non-aberrant messages (dubbed special messages) (Kuai *et al*, 2005) (Table 1). Our previous work established that all of these messages undergo active nuclear degradation by the exosome and its cofactor CTEXT without any participation by TRAMP (Maity *et al*, 2016). An assessment of the functional role of Nrd1p in the decay of export-incompetent messages collectively revealed that all the model aberrant export-defective mRNAs were stabilized dramatically in *nrd1-1* and *nrd1-2* strain backgrounds (Fig 3). The destabilization of *lys2-187* mRNA in *lys2-187* isogenic strains at 25°C (Fig 3A), nucleus-arrested *ACT1* and *CYC1* mRNA in *nup116*-Δ isogenic strains at 37°C (Fig 3B-C) and three export-incompetent special mRNAs *NCW2*, *SKS1* and *IMP3* in normal isogenic strains at 25°C (Fig 3D-F) were all rescued in the corresponding isogenic *rrp6*-Δ, *cbc1*-Δ, *nrd1-1*, and *nrd1-2* mutant yeast strains. As expected, the negative controls for this experiment, normal *CYC1* mRNA in *lys2-187* isogenic series (Fig. EV2C), and *ACT1* and *CYC1* mRNA in *nup116*-Δ isogenic strains at 25°C (Fig EV2D-E) did not display in any significant destabilization and concomitant stabilization by the *nrd1* mutations. Surprisingly and remarkably, none of the export-defective test messages displayed any steady-state enhancement at all in *nrd1*Δ^{CID} mutant isogenic strain (Fig 3). Consistent with the pattern of steady-state enhancement of the mutant *lys2-187* message in the *nrd1-1* and *nrd1-2* mutant strains, *lys2-187* strain also displayed a compromised growth in the SC-*lys* medium as compared to normal *LYS*$^{+}$ strain, which was rescued in all of the *lys2-187 nrd1-1*, *lys2-187 nrd1-2*, *lys2-187 rrp6*-Δ, *lys2-187 cbc1*-Δ yeast strains but not in a *lys2-187 nrd1*Δ^{CID} strain (Fig EV2F). Furthermore, the decay rate of *NCW2* message was found to be significantly (2-3 folds) diminished in *nrd1-1*, *nrd1-2* strains with concomitant increase in half-life values when compared to its decay rates in the wild-type and *nrd1*Δ^{CID} strains (Table 2, Fig 2F) thereby nicely correlated to the steady-state enhancement profile of this special message in these strains. Collectively, thus, these data

suggests that Nrd1p actively participates in the nuclear decay of all classes of export-defective transcripts. Interestingly, while the *nrd1-1*, *nrd1-2* mutations enhanced the steady-state levels of all of the export-inefficient transcripts, the *nrd1*Δ^{CID} mutation did not enhance their abundance at all thereby supporting the notion that *nrd1*Δ^{CID} protein is as efficient in supporting the degradation of the export defective messages as the wild type Nrd1p.

Next, we also established genetic epistasis between the core exosome/CTEXT components, Rrp6p, Cbc1p, and NNS component, Nrd1p, while evaluating if the core-exosome, CTEXT and NNS complex collectively act as a part of the same pathway. Findings from this experiment revealed that steady-state levels of the two special messages, *NCW2* and *SKS1* observed in the single mutant *rrp6-*Δ, *cbc1-*Δ and *nrd1-2* strains, did not further enhance in the double mutant *rrp6-*Δ *nrd1-2*, *cbc1-*Δ *nrd1-2* strains (Fig EV3A-B). Finally, while evaluating if the entire NNS complex (Nrd1p-Nab3p-Sen1p) collectively participates in the degradation of aberrant export-defective transcripts, we also observed that the steady-state levels of the special mRNAs, *IMP3*, *NCW2*, and *SKS1* mRNAs were dramatically stabilized in the yeast strains carrying *nab3-10* (four to eight folds) and *sen1-1* (two to five folds) mutations as compared to wild type strain (Fig EV4D-I). The normal *CYC1* mRNA, in contrast, neither display any destabilization nor stabilization in any of these strains (Fig EV4A-C). This data is thus consistent with the conclusion that Nrd1p-Nab3p-Sen1p together plays a crucial functional role in the decay of export defective special messages. Collectively, therefore, the findings from the experiments presented in this section, very strongly suggest that Nrd1p-Nab3p-Sen1p complex constitutes an integral component of the nuclear degradation machinery that targets all types of aberrant nuclear mRNAs (Table 3).

Strikingly, the *nrd1*Δ^{CID} mutation, unlike the *nrd1-1* and *nrd1-2* mutations, displayed a differential specificity towards the aberrant nuclear transcripts. While a dramatic effect of the *nrd1*Δ^{CID}

mutant was observed in stabilizing the transcription/assembly-, splice-, and 3′-processing-defective mRNAs, no stabilizing influence of this mutant was noted in case of export defective messages (Table 3). This observation suggests that although *nrd1*Δ^{CID}p is incapable of supporting the decay of the aberrant messages produced in the early and intermediate stages of mRNP biogenesis, it is able to support the rapid decay of the export-incompetent messages. Since the interaction of Nrd1p-RNAPII is abolished in the *nrd1*Δ^{CID} strain (Steinmetz & Brow, 1998; Steinmetz *et al*, 2001; Xu *et al*, 2009; Conrad *et al*, 2000; Vasiljeva & Buratowski, 2006), our data strongly indicates that the efficient degradation of aberrant mRNAs generated during transcript-elongation, splicing and 3′-end formation (early and intermediate stage of mRNP biogenesis) requires Nrd1p complex to be recruited co-transcriptionally onto these transcripts via RNAPII-CTD. For the rapid degradation of export-defective messages, in contrast, the CID domain appears dispensable, leading to the conclusion that *nrd1*Δ^{CID}p is still recruited onto the aberrant export-incompetent messages in an RNAPII-CTD independent manner and thereby support their nuclear decay. This conclusion, therefore, prompted us to look into the molecular insight into the co-transcriptional recruitment of the Nrd1p on various kinds of faulty messages to see if that is accompanied by its mRNA degradation activity and if its recruitment leads to their nuclear degradation.

RNAPII-dependent co-transcriptional recruitment of Nrd1p is vital for the exosome/TRAMP-dependent decay of the aberrant mRNAs derived during the early and intermediate stages of mRNA biogenesis.

We begin this section with a naïve question if Nrd1p recruitment on a faulty message is significantly higher in comparison to its normal functional counterpart. Consequently, the Nrd1p occupancy profiles of the *ACT1* and *CYC1* messages in THO mutant strains (representative of the

faulty messages stabilized by *nrd1*Δ^{CID} mutant) at 37°C (compared to their Nrd1p occupancy at 25°C) were found to be dramatically higher than those estimated at 25°C. Similarly, the Nrd1p occupancy of the export-incompetent message (representative of the defective mRNAs, which are not stabilized by *nrd1*Δ^{CID} mutant) *NCW2* at 25°C (compared to the Nrd1p occupancy on *CYC1* mRNA at 25°C) was significantly higher in comparison to typical message *CYC1* (Fig EV3D-F). This data supports the conclusion that a more copious amount of Nrd1p (and NNS complex) is selectively recruited on to faulty and otherwise unusual RNAs (such as special messages) in a co-transcriptional manner, which is targeted by the nuclear exosome. Next, we determined that occupancy profiles of truncated Nrd1p in yeast strains carrying the *nrd1-1* and *nrd1-2* are dramatically low on the *NCW2* and *SKS1* messages. This finding is consistent with the previous report that both these mutant proteins lack their RNA binding domain (RRM) (Vasiljeva & Buratowski, 2006; Conrad *et al*, 2000). Therefore, for all subsequent co-transcriptional recruitment experiments, we restricted ourselves in evaluating the Nrd1p occupancy profile in *NRD1*$^{+}$ and *nrd1*Δ^{CID} mutant yeast strains. Nevertheless, our data (i) indicates that Nrd1p recruitment onto aberrant messages perhaps marks these targets and (ii) hints at the possibility that initially, during the identification of aberrant messages, the primary distinction between the functional vs. aberrant is probably made by marking the faulty messages with the molecular "Nrd1p (or NNS)" mark.

Consequently, we determined the Nrd1p recruitment profile onto the two representative model mRNAs, each belonging to various classes of aberrant messages in isogenic yeast strains carrying either an *NRD1*$^{+}$ or *nrd1*Δ^{CID} allele. The final ChIP data using the primer sets corresponding to the central segment of each of the target mRNAs from individual ChIP sample is presented in Fig 4. Our findings revealed that, the representative transcription-elongation defective mRNAs in *hpr1-*Δ *NRD1*$^{+}$ strain, splice defective mRNAs in *prp2-1 NRD1*$^{+}$ strain and 3′-end processing-defective transcripts in

rna14-1 NRD1^{+} strain at the restrictive temperature of 37°C display a significantly high occupancy of Nrd1p in comparison to that estimated in corresponding *nrd1*Δ^{CID} isogenic strains (Figure 4A-C). Furthermore, we also observed that dramatically low recruitment of Nrd1p onto various aberrant messages observed in *nrd1*Δ^{CID} strains was not anyway associated with its low expression level since its expression levels in *NRD1*$^{+}$ and *nrd1*Δ^{CID} yeast strains were found to be very similar and comparable as shown in Fig EV3G. This observation thus clearly indicated that the Nrd1p occupancy onto the test mRNAs in an *nrd1*Δ^{CID} yeast strains is significantly lower because of the lack of association with the RNAPII-CTD, thereby justifies the view that Nrd1p recruitment on these aberrant messages derived in the early and intermediate phase of mRNP biogenesis is dependent on the RNAPII-CTD, which is vital for marking these messages as faulty.

Nuclear degradation of export-defective aberrant mRNAs generated in the late phase mRNP biogenesis requires Pcf11p-dependent recruitment of Nrd1p that precedes the recruitment of the Rrp6p/nuclear exosome.

Finally, we determined that the Nrd1p occupancy on the two representative export-defective special messages, *NCW2* and *SKS1* mRNAs in the wild type and *nrd1*Δ^{CID} mutant yeast strains at 25°C was very similar (Fig 4D), thereby strongly supporting the view that Nrd1p recruitment on export-defective messages (i) took place normally in an *nrd1*Δ^{CID} strain and supported their rapid decay, and (ii) does not require its CID domain, and hence it is independent of the RNAPII-dependent recruitment. Collectively, thus, we establish that Nrd1p (and NNS complex) participates in the nuclear degradation of all kinds of aberrant mRNA targets derived at various phases of mRNP biogenesis and its recruitment onto these aberrant messages is vital for their nuclear decay. Interestingly, however, the co-transcriptional recruitment of Nrd1p in the early/intermediate phase is strongly dictated by its interaction with RNAPII (via the interaction of the RNAPII CTD-Nrd1pCID domain). In contrast, its

recruitment onto the defective messages generated at the terminal phase of mRNP biogenesis is independent of RNAPII. To find out the cellular recruiter of Nrd1p onto the export-inefficient messages, we scrutinized into the literature in search of an ideal factor, which should be characterized by its ability (i) to support only the decay of export-defective messages but not the decay of other aberrant classes, (ii) to selectively promote the recruitment of Nrd1p on the model-export defective messages only, and (iii) to physically interact with Nrd1p.

A thorough search prompted us to postulate that, Pcf11p, a key component of cleavage and polyadenylation specific (CPSF) complex, which is involved in the transcription termination of poly(A)$^+$ RNAs may serve as a putative recruiter. Remarkably, Pcf11p also possesses a CID (CTD-interacting domain) like Nrd1p, and this protein interacts with RNAPII and many nascent mRNAs after being recruited by RNAPII via its CID (Amrani *et al*, 1997; Barilla *et al*, 2001; Licatalosi *et al*, 2002; Sadowski *et al*, 2003; Zhang *et al*, 2005). Most interestingly, Nrd1p, and Pcf11p were found to interact physically by affinity capture RNA method (Creamer *et al*, 2011) and genetically by dosage rescue (Singh *et al*, 2009). Our initial effort to test the Pcf11p as the possible recruiter of Nrd1p revealed that while a mutant yeast strain harboring a *pcf11-2* allele (Amrani *et al*, 1997) did not enhance the steady-state levels of two representative transcription-elongation/assembly-defective messages in THO mutant isogenic strain background, it firmly stabilized the two export-defective special messages, *NCW2* and *SKS1* mRNAs (Fig 5A-B), thereby strongly supporting our prediction. Consistent with this finding, a comparison of the Nrd1p occupancy profiles on the same group of representative messages displayed that while recruitment profile on the transcription-elongation assembly defective *ACT1* and *CYC1* messages remained unaltered in *pcf11-2* mutant yeast strain, it is significantly reduced on the *NCW2* and *SKS1* mRNAs in the same *pcf11-2* strain (Fig 5C-D). This finding is, thus, consistent with the conclusion that Pcf11p plays a vital functional role in the co-transcriptional recruitment of Nrd1p onto

the export-defective messages, thereby promoting their nuclear degradation by the Nrd1p/nuclear exosome.

Finally, we demonstrated that the Nrd1p recruitment on the aberrant export defective mRNAs leads to the further recruitment of the exosome component Rrp6p onto export-incompetent messages by showing that Rrp6p occupancy profiles on the two special mRNAs, *NCW2* and *SKS1* is very high in both the *NRD1*$^{+}$ and *nrd1*Δ^{CID} mutant strains, whereas, it is significantly low in *nrd1-1* and *nrd1-2* strains (Fig 5E). This data thus strongly support our conclusion that co-transcriptional recruitment of Nrd1p onto the export-defective aberrant messages (mediated by Pcf11p) is followed by the subsequent recruitment of the nuclear exosome, thereby stimulating their rapid nuclear decay. Thus, collectively, our experimental findings are consistent with the conclusion that the trimeric Nrd1p-Nab3p-Sen1p complex constitutes a vital and universal component of the nuclear decay and surveillance apparatus in *Saccharomyces cerevisiae* and its co-transcriptional recruitment is crucial for the nuclear degradation of the entire spectrum of aberrant mRNAs. We presented evidence that at least for the aberrant export defective messages, the co-transcriptional recruitment of this complex precedes the subsequent recruitment of the nuclear exosome for facilitating their degradation. Thus, the Nrd1p-Nab3p-Sen1p complex appears to serve as an exosome-specificity factor that co-transcriptionally recognizes the aberrant mRNAs very early in the transcription and mRNP biogenesis.

Although our previous work demonstrated a differential distribution of duty among the two exosomal cofactors, TRAMP and CTEXT, and their stage-specific recruitment on the diverse faulty messages (Maity *et al*, 2016), the mechanism of stage-specific recognition of distinct aberrant message is largely unknown. Consequently, despite being theoretically hypothesized previously (Vasiljeva & Buratowski, 2006; Kilchert *et al*, 2016), the existence of 'Exosome Specificity Factor' (ESF), and its universality and functionality remained elusive. Only recently, Nrd1p was demonstrated to facilitate

the exosomal degradation of Rho-induced transcription-elongation processing defective (Mosrin-Huaman *et al*, 2009) mRNPs in *Saccharomyces* cerevisiae (Honorine *et al*, 2011; Moreau *et al*, 2019). Although these study unraveled a key role of Nrd1p in the degradation of Rho-induced faulty messages, Nrd1p/NNS was neither demonstrated as the primary recruiter of Rrp6 nor its contribution in the degradation of other kinds of aberrant nuclear mRNAs was addressed.

Physical interaction between Nrd1p and the cap-binding component Cbc1p, (a major component of CTEXT) and exosome component Rrp6p (Vasiljeva & Buratowski, 2006) inspired us to address the functional role of NNS complex in the nuclear mRNA decay. This inspiration was further bolstered when TRAMP4 component Trf4p was reported to interact with Nrd1p (Tudek *et al*, 2014). Furthermore, we also addressed whether the NNS complex acts as an ESF and thereby controlling the recruitment of the nuclear exosome onto its target messages. As presented above, our results revealed that Nrd1p (and possibly NNS complex) participates in the degradation of all sorts of faulty mRNPs produced at different phases of mRNP maturation and the recruitment of Nrd1p (and possibly NNS) onto specific messages is vital for their decay. While the co-transcriptional recruitment of Nrd1p during transcription elongation, splicing, and 3′-end processing is carried out by RNAPII via RNAPII-CTD-Ser5-*NRD1*-CID interaction, its recruitment onto the export inefficient message is mediated by Pcf11p, via RNAPII-CTD-Ser2-*PCF11*-CID interaction (Table 4), thereby implying that in the terminal phase of mRNP biogenesis, Nrd1p-RNAPII is displaced by Pcf11p-RNAPII once the RNAPII is phosphorylated at Ser2. Substitution at the RNAPII-CTD is then followed by the recruitment of Nrd1p (NNS complex) on the aberrant mRNAs by Pcf11p. Alternatively, Pcf11p may directly recruit Nrd1p post-transcriptionally onto the export-defective messages without any involvement of RNAPII. Although it is not clear why Pcf11p is required for the recruitment of Nrd1p onto the export-defective message, it is possible that these messages may not have a strong association with RNAPII as they

perhaps originate after the cleavage/ polyadenylation reaction. At this stage, they appear to lose a strong association with RNAPII, while still remain attached to the transcription foci. This loose association necessitates the involvement of Pcf11p for their identification as aberrant RNA via the recruitment of Nrd1p. Future work would delineate this apparent mystery.

Nevertheless, our data hints at an exciting possibility that the NNS complex by acting as an ESF co-ordinate the recruitment of either TRAMP or CTEXT differentially onto their distinct subsets of faulty messages. Although the underlying mechanism is still elusive, Nrd1p recruitment via RNAPII Ser5CTD-*NRD1*-CID interaction appears very critical for the selective recruitment of TRAMP (to target transcription elongation- and splice-defective messages). In contrast, its recruitment via RNAPII Ser2CTD-*PCF11*-CID interaction seems vital for the recruitment of CTEXT (to target and degrade export defective messages). Indeed this conclusion explains our finding that the nuclear decay of the aberrantly long 3′-extended read-through transcripts requires the combined activity of TRAMP and CTEXT. These 3′-extended faulty transcripts are generated during the intermediate phase of mRNP biogenesis when the predominant population of RNAPII-CTD remains hyperphosphorylated consisting of both Ser5/Ser2 marks (Kim *et al*, 2010; Tietjen *et al*, 2010; Mayer *et al*, 2010). Since, both Nrd1p and Pcf11p remain associated with the hyperphosphorylated RNAPII-CTD having both Ser5-P/ Ser2-P mark (Vasiljeva *et al*, 2008; Kubicek *et al*, 2012; Barilla *et al*, 2001; Lunde *et al*, 2010), this situation subsequently recruits both TRAMP (Recruited directly by Nrd1p) and CTEXT (Recruited indirectly by Pcf11p) onto these read-through transcripts presumably in the long 3′-extended segments. This conclusion is supported by our observation that recruitment of Nrd1p onto these read-through messages in *nrd1*Δ^{CID} was not as low (about 40-50% compared to *NRD1*$^{+}$ strain, Fig 4C) as those found in the cases of transcription elongation-defective and splice-defective messages (about 5-20% compared to *NRD1*$^{+}$ strain, Fig 4A and B). This data thus strongly implied that in the *nrd1*Δ^{CID} yeast strain, the

remaining 40-50% of the recruited Nrd1p onto these 3′-extended faulty messages was carried out via Pcf11p dependent manner.

Our data imply that NNS complex qualifies well as a universal ESF by virtue of (i) exhibiting a uniform affinity to all categories of aberrant nuclear messages (ii) having an ability to identify and delineate a distinct set of aberrant message from a massive pool of cellular mRNAs via its increased occupancy of itself on these messages. This conclusion is strongly supported by the dramatically increased co-transcriptional recruitment observed onto the aberrant mRNA targets generated in THO mutant strains (e.g., mRNAs from *hpr1*-Δ at 37°C compared to 25°C, see Fig EV3D and E) or onto the special messages (*NCW2* vs. *CYC1*, see Fig EV4F). Although the molecular basis of RNAPII-dependent coordination of the selective Nrd1p recruitment onto a specific type of aberrant messages during various phases of transcription elongation and mRNP maturation events is currently unknown, this mystery leaves us with an opportunity to investigate further the insight into the distinguishing feature(s) of aberrant messages that Nrd1p recognizes and currently work in this direction is underway.

Materials and methods

Nomenclature, strains, media, and yeast genetics

Standard genetic nomenclature is used to designate wild-type alleles (e.g., *ACT1*, *CYC1*, *CYH2*, *LYS2*, *HPR1*), recessive mutant alleles (e.g., *lys2-187*, *nup116*-Δ, *nrd1-1*, *nrd1-2*, *nrd1*Δ^{CID}) and disruptants or deletions (e.g., *cbc1*::*TRP1*, *cbc1*-Δ, *rrp6*::*TRP1*, *rrp6*-Δ). An example of denoting a protein encoded by a gene is as follows: Nrd1p encoded by *NRD1*. The genotypes of *S. cerevisiae* strains used in this study are listed in **Table EV1**. Standard YPD, YPG, SC-Lys (lysine omission), and other omission media were used for testing and growth of yeast (Sherman, 1991). Yeast genetic analysis was carried out by standard procedures (Sherman, 1991).

Plasmids and oligonucleotides

The plasmids were either procured from elsewhere or were constructed in this laboratory using standard procedures. All the oligonucleotides were obtained commercially from Integrated DNA Technology. The plasmids and oligonucleotides used in this study are listed in **Tables EV2 and EV3**, respectively.

Plate Assay for suppressibility of the *lys2-187* mutation

A series of 10^{-1} dilution of suspension of 10^5 cells per ml were spotted on YPD, and lysine omission medium (SC-Lys) and the plates were incubated at 30°C for either 3 (for YPD) or 4-5 days (for Sc-Lys) medium followed by capturing the image of the cell growth as described previously (Das *et al*, 2006).

RNA analyses and determination of steady-state and decay rate of mRNAs

Total RNA was isolated as described earlier (Das *et al*, 2014) by harvesting appropriate yeast strains followed by extracting the cell suspension in the presence of phenol-chloroform-IAA (25:24:1) and glass bead. Following the extraction, the RNA was recovered by precipitation with RNAase-free ethanol. For the preparation of cDNA, total RNA was treated with DNase I (Fermentas Inc.,

Pittsburgh, PA, USA) to remove genomic DNA at 37◦C for 30 minutes. The reaction was stopped by adding 1µl of EDTA and incubating at 65°C for 10 minutes, followed by first-strand cDNA synthesis using Superscript Reverse Transcriptase (Invitrogen) using Random Primer (Bioline Inc.) by incubating the reaction mixture at 50°C for 30 minutes. Real-time qPCR analyses were performed with 2–3 ng of cDNA samples for *ACT1*, *CYC1*, *LYS2*, *NCW2*, *SKS1*, etc. and 30 ng for intron-containing splice defective messages, *ACT1* and *CYH2* in *prp2-1* strains to determine the steady-state levels as described previously (Das *et al*, 2014) decay rate of a specific mRNA was determined by the inhibition of global transcription with transcription inhibitor 1, 10-phenanthroline (Sigma-Aldrich) at 25°C or 37°C (as mentioned) and is described previously (Das *et al*, 2014). Briefly, the specific strain was grown at 25°C till mid-logarithmic phase (special messages), or an additional step was added for temperature-sensitive mutant (*hpr1*-Δ, *prp2-1*, *rna14-1*) of shifting the culture from 25°C to 37°C for 2 hours. This was followed by addition of 1, 10-Phenanthroline to the growing culture at a final concentration of 100 µg/mL and a shift in withdrawal of a 25 ml of aliquots of culture at various times after transcription shut off. Messenger RNA levels were quantified from cDNA by real-time PCR analysis and the signals associated with the specific messages were normalized against *SCR1* signals. The decay rates and half-lives of specific mRNAs were estimated with the regression analysis program (Graphpad Prism version 7.04) using a single exponential decay formula (assuming mRNA decay follows a first order kinetics), $y = 100e^{-bx}$ was used.

Real-Time PCR

Following the synthesis from total RNA samples, each cDNA was first quantified using Qubit®ds DNA HS Assay Kit (Life Technologies, USA) following their recommendation. 2 to 3 ng of quantified cDNA was used to quantify the levels of specific mRNAs such as *CYC1*, *ACT1*, *IMP3*, *NCW2*, and *LYS2*, etc. by qPCR assays by using target-specific primers and standard SYBR Green Technology

using Power SYBR® Green PCR Master Mix (Applied Biosystems). qPCR assays were run in triplicate and conducted using an Applied Biosystems StepOne™ real-time PCR system to determine the absolute quantification of individual target mRNAs. For each target either $\Delta\Delta^{-Ct}$ method was used, or purified DNA templates were prepared by PCR, followed by Gel purification and diluted serially to generate standard curves from 10^2 to 10^9copy number/reaction versus threshold cycle (C_t), determined from fluorescence by the StepOne™ software version 2.2.2 (Applied Biosystems). Standard curves were used to determine the amplification efficiencies ($E = 10^{(-1/n)}$, where n = slope of the standard curve) in SYBR Green assays as well as copy numbers of templates in experimental samples.

Chromatin Immunoprecipitation (ChIP) Assay

Chromatin preparation was essentially performed following the procedure described earlier (Keogh & Buratowski, 2004). The *NRD1*$^+$ and *nrd1*Δ^{CID} strains or *PCF11*$^+$ and *pcf11-2* strains in the different backgrounds were used for this study. Two fifty milliliters of cells grown till $OD_{600} \approx 0.5$ ($\approx 10^7$cells/ml) and were fixed with 1% formaldehyde for 20 min. The reaction was stopped by the addition of glycine, and the cells were washed and lysed with glass beads to isolate chromatin. The cross-linked chromatin was sheared by sonication to reduce average fragment size to ≈500bp. Chromatin-IP was carried using the ChIP assay kit (EZ-ChIP ™; Cat#17-295) from Merck Millipore. Immunoprecipitation of 120 µg Chromatin fractions (≈ 100µl) from each strain was performed using anti-Nrd1p antibody incubated overnight at 4◦C. Incubation with Protein G agarose bead was followed by washing and chromatin elution, the eluted supernatants and the input controls were incubated with Proteinase K for 1h at 37◦C followed by 5h at 65◦C to reverse cross-link the precipitated DNA from the complexes. DNA was purified using the DNA-clean up column provided with the kit. The immunoprecipitated DNAs (output) were quantified by real-time PCR (as mentioned above) using three sets of primers located along a specific genes coding sequence (5′-end, middle, and 3′-end) and

normalized to a half dilution of input DNA. Amplifications were done in duplicate for each sample (technical replicate), averages, and standard deviations were calculated based on three independent experiments (biological replicate).

Acknowledgements

We gratefully acknowledge Dr. Stephen Buratowski (Department of Biological Chemistry and Molecular Pharmacology, Harvard Medical School, Boston, MA, USA) for kindly sharing *nrd1-1*, *nrd1-2*, *nrd1*Δ^{CID}, *sen1-1*mutant strains, anti-Nrd1antibody, and various *NRD1* plasmids. We also acknowledge Dr. Maurice Swanson (University of Florida, Gainesville, FL, USA) for *nab3-10*, Dr. Jeffry Corden (Johns Hopkins School of Medicine, Baltimore, MD, USA) for, Dr. Athar Ansari (Wayne State University, Michigan, USA) for the *pcf11-2* mutant yeast strains, and Dr. Scott Butler for providing us with the Anti-Rrp6p antibody (University of Rochester, Rochester, NY, USA). We thank Dr. Satarupa Das, Dr. Arindam Chakraborty, and the members of the Das Laboratory for critically reading this manuscript. We also thank the anonymous reviewers for their critical comments and constructive suggestion, which enriched this manuscript. Please add anybody if you think that I am missing anyone.

Funding

This investigation was supported by research grants from DBT (Award No. BT/PR27917/BRB/10/ 1673/2018) and Jadavpur University (RUSA 2.0 Research Grant to BD). PS is supported by a State Research Fellowship from the Government of West Bengal, West Bengal, India.

References

Allmang C, Mitchell P, Petfalski E & Tollervey D (2000) Degradation of ribosomal RNA precursors by the exosome. *Nucleic Acids Res* **28:** 1684–1691 Available at: http://www.ncbi.nlm.nih.gov/pubmed/10734186

Amrani N, Minet M, Wyers F, Dufour ME, Aggerbeck LP & Lacroute F (1997) PCF11 encodes a third protein component of yeast cleavage and polyadenylation factor I. *Mol. Cell. Biol.* **17:** 1102–1109

Barilla D, Lee BA & Proudfoot NJ (2001) Cleavage/polyadenylation factor IA associates with the carboxyl-terminal domain of RNA polymerase II in Saccharomyces cerevisiae. *Proc. Natl. Acad. Sci.* **98:** 445–450

Birse CE, Minvielle-Sebastia L, Lee BA, Keller W & Proudfoot NJ (1998) Coupling termination of transcription to messenger RNA maturation in yeast. *Science (80-.).* **280:** 298–301 Available at: http://www.ncbi.nlm.nih.gov/pubmed/9535662

Bousquet-Antonelli C, Presutti C & Tollervey D (2000) Identification of a regulated pathway for nuclear pre-mRNA turnover. *Cell* **102:** 765–775 Available at: http://www.ncbi.nlm.nih.gov/pubmed/11030620

Bresson S, Tuck A, Staneva D & Tollervey D (2017) Nuclear RNA Decay Pathways Aid Rapid Remodeling of Gene Expression in Yeast. *Mol Cell* **65:** 787-800 e5 Available at: http://www.ncbi.nlm.nih.gov/pubmed/28190770

Butler JS (2002) The yin and yang of the exosome. *Trends Cell Biol* **12:** 90–96 Available at: http://www.ncbi.nlm.nih.gov/pubmed/11849973

Cloutier SC, Ma WK, Nguyen LT & Tran EJ (2012) The DEAD-box RNA helicase Dbp2 connects RNA quality control with repression of aberrant transcription. *J. Biol. Chem.* **287:** 26155–26166

Conrad NK, Wilson SM, Steinmetz EJ, Patturajan M, Brow DA, Swanson MS & Corden JL (2000) A

yeast heterogeneous nuclear ribonucleoprotein complex associated with RNA polymerase II. *Genetics* **154:** 557–571 Available at: http://www.ncbi.nlm.nih.gov/pubmed/10655211

Creamer TJ, Darby MM, Jamonnak N, Schaughency P, Hao H, Wheelan SJ & Corden JL (2011) Transcriptome-wide binding sites for components of the Saccharomyces cerevisiae non-poly(A) termination pathway: Nrd1, Nab3, and Sen1. *PLoS Genet.* **7:**

Das B, Butler JS & Sherman F (2003) Degradation of normal mRNA in the nucleus of Saccharomyces cerevisiae. *Mol. Cell. Biol.* **23:**

Das B, Das S & Sherman F (2006) Mutant LYS2 mRNAs retained and degraded in the nucleus of Saccharomyces cerevisiae. *Proc. Natl. Acad. Sci. U. S. A.* **103:**

Das B, Guo Z, Russo P, Chartrand P & Sherman F (2000) The role of nuclear cap binding protein Cbc1p of yeast in mRNA termination and degradation. *Mol. Cell. Biol.* **20:**

Das S & Das B (2013) MRNA quality control pathways in Saccharomyces cerevisiae. *J. Biosci.* **38:**

Das S, Saha U & Das B (2014) Cbc2p, Upf3p and eIF4G are components of the DRN (Degradation of mRNA in the Nucleus) in Saccharomyces cerevisiae. *FEMS Yeast Res.* **14:**

Eichinger CS & Jentsch S (2010) Synaptonemal complex formation and meiotic checkpoint signaling are linked to the lateral element protein red1. *Proc. Natl. Acad. Sci. U. S. A.* **107:** 11370–11375

Halbach F, Reichelt P, Rode M & Conti E (2013) The yeast ski complex: crystal structure and RNA channeling to the exosome complex. *Cell* **154:** 814–826 Available at: http://www.ncbi.nlm.nih.gov/pubmed/23953113

Hardwick SW & Luisi BF (2013) Rarely at rest: RNA helicases and their busy contributions to RNA degradation, regulation and quality control. *RNA Biol* **10:** 56–70 Available at: http://www.ncbi.nlm.nih.gov/pubmed/23064154

Honorine R, Mosrin-Huaman C, Hervouet-Coste N, Libri D & Rahmouni AR (2011) Nuclear mRNA

quality control in yeast is mediated by Nrd1 co-transcriptional recruitment, as revealed by the targeting of Rho-induced aberrant transcripts. *Nucleic Acids Res* **39:** 2809–2820 Available at: http://www.ncbi.nlm.nih.gov/pubmed/21113025

Keogh MC & Buratowski S (2004) Using chromatin immunoprecipitation to map cotranscriptional mRNA processing in Saccharomyces cerevisiae. *Methods Mol. Biol.* **257:** 1–16

Kilchert C, Wittmann S & Vasiljeva L (2016) The regulation and functions of the nuclear RNA exosome complex. *Nat Rev Mol Cell Biol* **17:** 227–239 Available at: http://www.ncbi.nlm.nih.gov/pubmed/26726035

Kim H, Erickson B, Luo W, Seward D, Graber JH, Pollock DD, Megee PC & Bentley DL (2010) Gene-specific RNA polymerase II phosphorylation and the CTD code. *Nat. Struct. Mol. Biol.* **17:** 1279–1286

Kong KYE, Tang HMV, Pan K, Huang Z, Lee THJ, Hinnebusch AG, Jin DY & Wong CM (2014) Cotranscriptional recruitment of yeast TRAMP complex to intronic sequences promotes optimal pre-mRNA splicing. *Nucleic Acids Res.* **42:** 643–660

Kuai L, Das B & Sherman F (2005) A nuclear degradation pathway controls the abundance of normal mRNAs in Saccharomyces cerevisiae. *Proc. Natl. Acad. Sci. U. S. A.* **102:**

Kubicek K, Cerna H, Holub P, Pasulka J, Hrossova D, Loehr F, Hofr C, Vanacova S & Stefl R (2012) Serine phosphorylation and proline isomerization in RNAP II CTD control recruitment of Nrdl. *Genes Dev.* **26:** 1891–1896

Libri D, Dower K, Boulay J, Thomsen R, Rosbash M & Jensen TH (2002) Interactions between mRNA export commitment, 3'-end quality control, and nuclear degradation. *Mol Cell Biol* **22:** 8254–8266 Available at: http://www.ncbi.nlm.nih.gov/pubmed/12417728

Licatalosi DD, Geiger G, Minet M, Schroeder S, Cilli K, McNeil JB & Bentley DL (2002) Functional

interaction of yeast pre-mRNA 3′ end processing factors with RNA polymerase II. *Mol. Cell* **9:** 1101–1111

Lunde BM, Reichow SL, Kim M, Suh H, Leeper TC, Yang F, Mutschler H, Buratowski S, Meinhart A & Varani G (2010) Cooperative interaction of transcription termination factors with the RNA polymerase II C-terminal domain. *Nat. Struct. Mol. Biol.* **17:** 1195–1201

Maity A, Chaudhuri A & Das B (2016) DRN and TRAMP degrade specific and overlapping aberrant mRNAs formed at various stages of mRNP biogenesis in Saccharomyces cerevisiae. *FEMS Yeast Res.* **16:**

Mayer A, Lidschreiber M, Siebert M, Leike K, Söding J & Cramer P (2010) Uniform transitions of the general RNA polymerase II transcription complex. *Nat. Struct. Mol. Biol.* **17:** 1272–1278

Minvielle-Sebastia L & Keller W (1999) mRNA polyadenylation and its coupling to other RNA processing reactions and to transcription. *Curr Opin Cell Biol* **11:** 352–357 Available at: http://www.ncbi.nlm.nih.gov/pubmed/10395555

Mitchell et al. 1997.pdf

Mitchell P (2014) Exosome substrate targeting: the long and short of it. *Biochem Soc Trans* **42:** 1129–1134 Available at: http://www.ncbi.nlm.nih.gov/pubmed/25110014

Moreau K, Le Dantec A, Mosrin-Huaman C, Bigot Y, Piégu B & Rahmouni AR (2019) Perturbation of mRNP biogenesis reveals a dynamic landscape of the Rrp6-dependent surveillance machinery trafficking along the yeast genome. *RNA Biol.* **16:** 879–889

Mosrin-Huaman C, Honorine R & Rahmouni AR (2009) Expression of Bacterial Rho Factor in Yeast Identifies New Factors Involved in the Functional Interplay between Transcription and mRNP biogenesis. *Mol. Cell. Biol.* **29:** 4033–4044

Parker R (2012) RNA degradation in Saccharomyces cerevisae. *Genetics* **191:** 671–702 Available at:

http://www.ncbi.nlm.nih.gov/pubmed/22785621

Plumpton M, McGarvey M & Beggs JD (1994) A dominant negative mutation in the conserved RNA helicase motif 'SAT' causes splicing factor PRP2 to stall in spliceosomes. *EMBO J* **13:** 879–887 Available at: http://www.ncbi.nlm.nih.gov/pubmed/8112301

Proudfoot N (2000) Connecting transcription to messenger RNA processing. *Trends Biochem Sci* **25:** 290–293 Available at: http://www.ncbi.nlm.nih.gov/pubmed/10838569

Rougemaille M, Gudipati RK, Olesen JR, Thomsen R, Seraphin B, Libri D & Jensen TH (2007) Dissecting mechanisms of nuclear mRNA surveillance in THO/sub2 complex mutants. *EMBO J* **26:** 2317–2326 Available at: http://www.ncbi.nlm.nih.gov/pubmed/17410208

Sadowski M, Dichtl B, Hübner W & Keller W (2003) Independent functions of yeast Pcf11p in pre-mRNA 3′ end processing and in transcription termination. *EMBO J.* **22:** 2167–2177

Schmidt K & Butler JS (2013) Nuclear RNA surveillance: role of TRAMP in controlling exosome specificity. *Wiley Interdiscip Rev RNA* **4:** 217–231 Available at: http://www.ncbi.nlm.nih.gov/pubmed/23417976

Sherman F (1991) Getting Started with Yeast. *Methods Enzymol.* **194:** 3–21

Singh N, Ma Z, Gemmill T, Wu X, DeFiglio H, Rossettini A, Rabeler C, Beane O, Morse RH, Palumbo MJ & Hanes SD (2009) The Ess1 Prolyl Isomerase Is Required for Transcription Termination of Small Noncoding RNAs via the Nrd1 Pathway. *Mol. Cell* **36:** 255–266

Steinmetz EJ & Brow DA (1998) Control of pre-mRNA accumulation by the essential yeast protein Nrd1 requires high-affinity transcript binding and a domain implicated in RNA polymerase II association. *Proc Natl Acad Sci U S A* **95:** 6699–6704 Available at: http://www.ncbi.nlm.nih.gov/pubmed/9618475

Steinmetz EJ, Conrad NK, Brow DA & Corden JL (2001) RNA-binding protein Nrd1 directs poly(A)-

independent 3’-end formation of RNA polymerase II transcripts. *Nature* **413:** 327–331 Available at: http://www.ncbi.nlm.nih.gov/pubmed/11565036

Strasser K, Masuda S, Mason P, Pfannstiel J, Oppizzi M, Rodriguez-Navarro S, Rondon AG, Aguilera A, Struhl K, Reed R & Hurt E (2002) TREX is a conserved complex coupling transcription with messenger RNA export. *Nature* **417:** 304–308 Available at: http://www.ncbi.nlm.nih.gov/pubmed/11979277

Tietjen JR, Zhang DW, Rodríguez-Molina JB, White BE, Akhtar MS, Heidemann M, Li X, Chapman RD, Shokat K, Keles S, Eick D & Ansari AZ (2010) Chemical-genomic dissection of the CTD code. *Nat. Struct. Mol. Biol.* **17:** 1154–1161

Torchet C, Bousquet-Antonelli C, Milligan L, Thompson E, Kufel J & Tollervey D (2002) Processing of 3’-extended read-through transcripts by the exosome can generate functional mRNAs. *Mol Cell* **9:** 1285–1296 Available at: http://www.ncbi.nlm.nih.gov/pubmed/12086625

Tudek A, Porrua O, Kabzinski T, Lidschreiber M, Kubicek K, Fortova A, Lacroute F, Vanacova S, Cramer P, Stefl R & Libri D (2014) Molecular basis for coordinating transcription termination with noncoding RNA degradation. *Mol Cell* **55:** 467–481 Available at: http://www.ncbi.nlm.nih.gov/pubmed/25066235

Vasiljeva L & Buratowski S (2006) Nrd1 interacts with the nuclear exosome for 3’ processing of RNA polymerase II transcripts. *Mol Cell* **21:** 239–248 Available at: http://www.ncbi.nlm.nih.gov/pubmed/16427013

Vasiljeva L, Kim M, Mutschler H, Buratowski S & Meinhart A (2008) The Nrd1-Nab3-Sen1 termination complex interacts with the Ser5-phosphorylated RNA polymerase II C-terminal domain. *Nat Struct Mol Biol* **15:** 795–804 Available at: http://www.ncbi.nlm.nih.gov/pubmed/18660819

Wente SR & Blobel G (1993) A temperature-sensitive NUP116 null mutant forms a nuclear envelope seal over the yeast nuclear pore complex thereby blocking nucleocytoplasmic traffic. *J. Cell Biol.* **123:** 275–284

Xu Z, Wei W, Gagneur J, Perocchi F, Clauder-Munster S, Camblong J, Guffanti E, Stutz F, Huber W & Steinmetz LM (2009) Bidirectional promoters generate pervasive transcription in yeast. *Nature* **457:** 1033–1037 Available at: http://www.ncbi.nlm.nih.gov/pubmed/19169243

Yonaha M & Proudfoot NJ (2000) Transcriptional termination and coupled polyadenylation in vitro. *EMBO J* **19:** 3770–3777 Available at: http://www.ncbi.nlm.nih.gov/pubmed/10899130

Zenklusen D, Vinciguerra P, Wyss JC & Stutz F (2002) Stable mRNP formation and export require cotranscriptional recruitment of the mRNA export factors Yra1p and Sub2p by Hpr1p. *Mol Cell Biol* **22:** 8241–8253 Available at: http://www.ncbi.nlm.nih.gov/pubmed/12417727

Zhang Z, Fu J & Gilmour DS (2005) CTD-dependent dismantling of the RNA polymerase II elongation complex by the pre-mRNA 3′-end processing factor, Pcf11. *Genes Dev.* **19:** 1572–1580

Table 1: Various types of aberrant mRNA substrates, generated progressively during mRNP biogenesis, the specificity of the decay apparatus to degrade them, and their representative model mRNAs used in this study

Stages of mRNP Biogenesis	mRNP Biogenesis events	Nature of Aberrant mRNAs	Specificity of Core Exosome ($EXO11^{Dis3p+Rrp6p}$)	Specificity of TRAMP	Specificity of CTEXT	Yeast mutant strain background used for this study	Representative mRNAs evaluated
Early	Transcription	Transcription assembly defective	+	+	–	*hpr1*-Δ	*ACT1*, *CYC1*
	Splicing	Intron-containing splice defective	+	+	–	*prp2-1*	pre-*ACT1*, pre-*CYH2*
Intermediate	3′-end Processing	Aberrant transcription termination read-through transcripts with long 3′-Extension	+	+	+	*rna14-1*	*LYS2*, *CYC1*
						lys2-187 mRNA	*lys2-187*
Late	Nuclear Export	Export Defective	+	–	+	nucleus-retained mRNAs in *nup116*-Δ strain	*ACT1* *CYC1*
						non-aberrant special mRNAs	*IMP3* *NCW2* *SKS1*

Table 2: Half-life values of various aberrant mRNAs in different yeast strains carrying various mutant alleles in *NRD1* gene in the backgrounds of transcription-elongation-defect (*hpr1*-Δ), splicing-defect (*prp2-1*) and 3′-end formation (*rna14-1*) defect

Yeast Strain defective in	Target aberrant message	Half-life (in minutes) of specific target messages in various *nrd1* mutant strains			
		Wild Type	***nrd1-1***	***nrd1-2***	***nrd1*Δ^{CID}**
Transcription-Elongation (*hpr1*-Δ)	*ACT1*	10.37	20.6	20.15	29.19
	CYC1	10.22	29.94	19.77	29.96,
Splicing (*prp2-1*)	pre-*CYH2*	9.925	20.15	20.09	19.85
3′-end Processing (*rna14-1*)	*LYS2*	10.24	20.06	19.75	19.86
	CYC1	10.37	20.06	20.15	29.19
None	*NCW2*	10.11	19.82	19.87	9.952

Table 3: Specificity of Nrd1p in the decay of various aberrant nuclear mRNA targets examined in this study and the effect of various *nrd1* mutants in their stabilization

Stages of Nuclear mRNP Biogenesis	mRNP Biogenesis event	Nature of aberrant mRNAs	Involvement of Nrd1p	Effects of different *nrd1* mutations in the stabilization of		
				nrd1-1	***nrd1-2***	***nrd1*Δ^{CID}**
Early	Transcription	Transcription-Elongation defective	+	+	+	+
	Splicing	Splicing defective Intron-containing	+	+	+	+
Intermediate	3′-end Processing	Aberrant transcription termination read-through transcripts with long 3′-Extension	+	+	+	+
Late	Nuclear Export	Export Defective	+	+	+	–

Table 4: Recruitment profiles of Nrd1p on various aberrant nuclear mRNA targets

Recruiter	Nrd1p Recruitment			
	Transcription-Assembly- defective	Intron-containing Splice-defective	Transcription-termination defective read-through transcripts with long 3′-Extension	Export-defective
RNAPII	+	+	+	–
Pcf11p	–	–	–	+

Legends to the Figures

Figure 1. Nrd1p actively participates in the degradation of aberrant mRNPs generated in transcription-elongation-(*hpr1*-Δ) (A), splice-(*prp2-1*) (B) and 3′-end processing-(*rna14-1*) defective (C) yeast strains. (A) Scatter plot revealing the relative abundance of transcription assembly-defective *ACT1* and *CYC1* mRNAs at 37°C in the indicated isogenic *hpr1*-Δ strains. The mean normalized level of each target mRNA estimated in the $HPR1^+$ sample was set to 1. P-value was estimated with respect to the steady-state levels of the transcript in *hpr1*-Δ yeast strain (B) Scatter plot revealing the relative abundance of two intron-containing precursor pre-*ACT1* and pre-*CYH2* transcripts at 37°C in the indicated isogenic *prp2-1* strains. The normalized value of each pre-mRNA signal from *prp2-1* samples was set to 1 as pre-mRNAs are not reliably detectable in $PRP2^+$ strain. (C) Scatter plot revealing the relative levels of 3′-extended transcripts of *LYS2* and *CYC1* genes in the isogenic *rna14-1* strains. Normalized values of extended *CYC1* and *LYS2* mRNA samples from *rna14-1* strain at 37°C was set to 1 as read-through mRNAs are not reliably detectable in *RNA14+* strain.

For all of the above experiments, three independent samples of random-primed cDNA (biological replicates, N=3) were prepared from indicated strains, pre-grown at 25°C followed by a 2-h shift for *hpr1*-Δ (A) and 3-h shift for *prp2-1* (B) and *rna14-1* (C) yeast strains at 37°C before subjected to qRT-PCR analysis using gene-specific primer sets for respective target mRNAs. For transcription assembly defective *ACT1* and *CYC1* mRNAs in (A), the primer sets corresponding to the coding regions of each message was used. Approximate locations of the primer pairs and the corresponding amplicons of the pre-*ACT1*, pre-*CYH2* precursor mRNAs in the *prp2-1* isogenic background shown in (B) and those of the 3′-extended read through *LYS2*, and *CYC1* mRNAs in the *rna14-1* isogenic background shown in (C) are schematically shown in Figure S2A. Transcript copy numbers/3 ng cDNA for *hpr1*-Δ, and *rna14-1* strains and 50 ng for *prp2-1* strains were normalized to 18S rRNA signals obtained from respective samples and are shown as means ± SE. The statistical significance of difference, as reflected in the ranges of P values estimated from Student's two-tailed t-test for a given pair of test strains for each message, is presented with the following symbols, $*$ <0.05, $**$<0.005 and $***$<0.001, NS, not significant.

Figure 2. Decay kinetics of representative transcription-elongation-defective (A-B), splice-defective (C), 3′-end processing-defective (D-E) messages at 37°C and export-defective special *NCW2* (F) mRNA at 25°C in the wild type and yeast strains harboring *nrd1-1, nrd1-2,* and

***nrd1*Δ^{CID} mutations.** Decay rates of (A-B) transcription assembly defective *ACT1* and *CYC1* mRNAs in isogenic *hpr1*-Δ strains, (C) intron-containing pre-*CYH2* mRNA in isogenic *prp2-1* strains, (D-E) 3′-end extended read-through *LYS2* and *CYC1* mRNAs in isogenic *rna14-1* strains, and (F) nucleus-retained special *NCW2* mRNA in the corresponding isogenic wild-type (orange line), *nrd1-1* (blue line), *nrd1-2* (pink line), *nrd1*Δ^{CID} (green line) strains. Decay rates were determined by qRT-PCR analysis from three independent samples of 2 ng cDNA (biological replicates, N=3) extracted from yeast strains harvested at various times following the treatment of the cells with transcription-inhibitor 100 μg/mL 1, 10-phenanthroline. qRT-PCR signals were normalized to *SCR1* RNA signals obtained from the same cDNA samples, and the normalized signals (mean values ± SD from three biological replicates, N = 3) from each time point were presented as the fraction of remaining RNA (with respect to normalized signals at 0 minute, which was set to 1) as a function of time of incubation in the presence of 1,10-phenanthroline.

Figure 3. Rapid nuclear decay of a variety of export-defective messages is rescued by *nrd1-1* and *nrd1-2* mutations, but not by *nrd1*Δ^{CID} mutation. (A) Relative steady-state levels of normal *LYS2* and export-defective *lys2-187* mRNAs at 25°C in the indicated isogenic yeast strains. The normalized value of the *LYS2* transcript from the *LYS2*$^{+}$ sample was set to 1. P-value was estimated with respect to the steady-state levels of the transcript in the *lys2-187* yeast strain (B-C) Scatter plot, revealing the relatively steady-state levels of nucleus-retained *ACT1* (B) and *CYC1* at 37°C (C) in the indicated isogenic *nup116*-Δ mutant strains. The normalized value of these transcripts from the *nup116*-Δ sample was set to 1. (D-F) Relative steady-state levels of three export inefficient special mRNAs, *IMP3* (D), *NCW2* (E) and *SKS1* (F), at 25°C in a wild type, *rrp6*-Δ, *cbc1*-Δ, *nrd1-1*, *nrd1-2*, and *nrd1*Δ^{CID} strains. The normalized value of each specific mRNAs from the wild-type sample was set to 1.

For all the above experiments, three independent samples of random-primed cDNA (biological replicates, N = 3) samples were prepared from the indicated isogenic strains grown at 25°C for isogenic *lys2-187* strains (A), pre-grown at 25C° followed by a 2-h shift to 37°C for *nup116*-Δ isogenic strains (B-C) and grown at 25°C for the normal isogenic strains (D-F) before subjecting them to real-time qPCR analysis using primer sets specific for each mRNA. Transcript copy numbers/3 ng cDNA for *lys2-187* strains, copy numbers/2 ng cDNA of other strain backgrounds were normalized to *SCR1* RNA levels in respective samples and are shown as means ± SE. The statistical significance of difference, as

reflected in the ranges of P values estimated from Student's two-tailed t-test for a given pair of test strains for each message, is presented with the following symbols, ∗ <0.05, ∗∗<0.005 and ∗∗∗<0.001, NS, not significant.

Figure 4. The co-transcriptional recruitment of Nrd1p lacking the *CID* domain is drastically impaired on (A) transcription assembly-defective, (B) splice-defective and (C) 3′-extended aberrant messages in comparison to full-length Nrd1p but remains unaltered on (D) export-defective special messages. Occupancy profile of full-length Nrd1p and Nrd1p lacking its *CID* domain of the (A) transcription-assembly-defective *ACT1* and *CYC1* mRNAs at 37°C in isogenic *hpr1*-Δ and *hpr1*-Δ *nrd1ΔCID* strains, (B) splice-defective intron-containing pre-*ACT1* and pre-*CYH2* at 37ºC in isogeneic *prp2-1* and *prp2-1 nrd1ΔCID* strains (C) 3′-extended read-through *CYC1* and *LYS2* transcripts at 37ºC in *rna14-1* and *rna14-1 nrd1ΔCID* strains and (D) nucleus-arrested special messages *NCW2* and *SKS1* at 25ºC in wild-type (*NRD1*$^{+}$) and *nrd1ΔCID* strains. Fragmented and cross-liked chromatin preparation was conducted from indicated strains at a specific temperature from three independent biological replicates (N=3) followed by the immunoprecipitation of the chromatin samples using specific Nrd1p antibody. Immunoprecipitated DNA was recovered as mentioned in materials and methods before qPCR analyses using the primer sets specific for the middle region of ORF of each target mRNA. Mean normalized qPCR signals ± SD from the immunoprecipitated (output) DNA to the mean qPCR signal obtained from the total chromatin (input) DNA of each sample obtained from three experiments are presented as scattered plot. The statistical significance of difference, as reflected in the ranges of p-values estimated from Student's two-tailed t-tests for a given pair of test strains for each message, is presented with the following symbols, * <0.05, **<0.005 and ***<0.001, NS, not significant.

Figure 5. Pcf11p actively contributes to the rapid nuclear decay of export-defective special messages by recruiting the Nrd1p that leads to the further recruitment of Rrp6p onto them. (A-B) Scatter plot revealing the relative steady-state levels of (A) two transcription assembly-defective *ACT1* and *CYC1* mRNAs in the indicated isogenic *hpr1*-Δ, *hpr1*-Δ *rrp6*-Δ, *hpr1*-Δ *cbc1*-Δ and *hpr1*-Δ *pcf11-2* strains and (B) two export-inefficient special mRNAs *NCW2* and *SKS1* in isogenic wild-type (*PCF11*$^{+}$), *rrp6*-Δ, *cbc1*-Δ and *pcf11-2* strains. In both cases, the normalized values of every target mRNA from the wild-type samples was set to 1. Normalized qRT-PCR signals (Mean ± SE) from

three independent biological replicates are presented as scatter plots, as described above. (C-D) co-transcriptional recruitment profiles of Nrd1p on (C) transcription assembly-defective *ACT1* and *CYC1* messages at 37°C in isogenic *hpr1*-Δ and *hpr1*-Δ *pcf11-2* strains, and (D) two export-incompetent special messages in *NCW2* and *SKS1* at 25°C in an isogenic wild-type and *pcf11-2* strains. (E) Occupancy profiles of Rrp6p on the two special mRNAs *NCW2* and S*KS1* at 25°C in the indicated isogenic wild-type (*NRD1*$^{+}$), *nrd1-1*, *nrd1-2*, and *nrd1*Δ^{CID} yeast strains. All immunoprecipitations using specific Nrd1p or Rrp6p antibody followed by the recovery of the precipitated DNA and qPCR analyses were performed exactly as described in materials and methods and the legend of Figure 4.

Expanded View Tables

Table EV1: List and Genotypes of Yeast Strains used in this study

Strain No.	Complete genotype	Abbreviated Genotype	Reference
yBD148	*MATa; ura3-52; leu2-3,112; trp1-1; his3-11,15; nrd1Δ::HIS3; lys2Δ2; ade2-1; met2Δ1, can1-100 [pRS316NRD1 (NRD1, URA3, CEN)]*	*HPR1*$^{+}$	Vasiljeva & Buratowski, 2006
yBD281	*MATa; ura3-52; leu2-3,112; trp1-1; his3-11,15; nrd1Δ::HIS3; lys2Δ2; ade2-1; met2Δ1, can1-100 [pRS316NRD1 (NRD1, URA3, CEN)] hpr1::LEU2*	*hpr1Δ*	This Study[¥]
yBD282	*MATa ura3-52 leu2-3,112 trp1-1 his3-11,15 nrd1::HIS3 lys2Δ2 ade2-1 met2Δ1 can1-100, (pRS 316 NRD1(NRD1, URA3,CEN)) rrp6::TRP1 hpr1::LEU2*	*hpr1Δrrp6Δ*	This Study[¥]
yBD283	*MATa; ura3-52; leu2-3,112; trp1-1; his3-11,15; nrd1Δ::HIS3; lys2Δ2; ade2-1; met2Δ1, can1-100 [pRS316NRD1 (NRD1, URA3, CEN)]; cbc1Δ::TRP1 hpr1::LEU2*	*hpr1Δcbc1Δ*	This Study[¥]
yBD330	*MATa ura3-52 leu2-3,112 trp1-1 his3-11,15 nrd1::HIS3 lys2Δ2 ade2-1 met2Δ1 can1-100, (pRS 424nrd1-1(nrd1-1, TRP1, 2μ ori)) hpr1::LEU2*	*hpr1Δnrd1-1*	This Study[¥]
yBD284	*MATa; ura3-52; leu2-3,112; trp1-1; his3-11,15; nrd1Δ::HIS3; lys2Δ2; ade2-1; met2Δ1, can1-100; [pRS424nrd1-2 (nrd1-2, TRP1, 2 μ ori)] hpr1::LEU2*	*hpr1Δnrd1-2*	This Study[¥]
yBD331	*MATa; ura3-52; leu2-3,112; trp1-1; his3-11,15;nrd1Δ::HIS3; lys2Δ2; ade2-1; met2Δ1, can1-100; [pRS314NRD1Δ39-169 (nrd1ΔCID(39-169), TRP1,CEN)]hpr1::LEU2*	*hpr1Δ nrd1ΔCID*	This Study[¥]
yBD70	*MAT a ade2-1 his3 ura3 leu2 trp1 prp2-1*	*prp2-1*	Bousquet-Antonelli et al, 2000
yBD77	*MAT a ade2 his3 ura3 leu2 trp1 prp2-1rrp6::URA3*	*prp2-1rrp6-Δ*	Bousquet-Antonelli et al, 2000
yBD76	*MAT a ade2 his3 ura3 leu2 trp1 prp2-1cbc1::URA3*	*prp2-1cbc1-Δ*	Bousquet-Antonelli et al, 2000
yBD382	*MAT a ade2-1 his3 ura3 leu2 trp1 prp2-1(pRS 424nrd1-2(nrd1-2, TRP1, 2μ ori))*	*prp2-1nrd1-1*	This Study[¥]
yBD381	*MAT a ade2-1 his3 ura3 leu2 trp1 prp2-1(pRS 424nrd1-1(nrd1-1, TRP1, 2μ ori))*	*prp2-1nrd1-2*	This Study[¥]
yBD383	*MAT a ade2-1 his3 ura3 leu2 trp1 prp2-1[pRS314NRD1Δ39-169 (nrd1ΔCID(39-169), TRP1,CEN)]*	*prp2-1nrd1ΔCID*	This Study[¥]
yBD151	*MATα; ura3-1; trp1-1; rna14-1*	*rna14-1*	Vasiljeva & Buratowski, 2006
yBD152	*MATα; ura3-1; trp1-1; rna14-1; rrp6Δ::KANMX*	*rna14-1 rrp6-Δ*	Vasiljeva & Buratowski, 2006
yBD354	*MATα; ura3-1; trp1-1; rna14-1; cbc1::hisG URA3 hisG (Blaster)*	*rna14-1 cbc1-Δ*	This Study[¥]
yBD153	*MATα; ura3-1; trp1-1; rna14-1; nrd1Δ::KANMX; [pRS424nrd1-1 (nrd1-1, TRP1, 2 μ ori)]*	*rna14-1 nrd1-1*	Vasiljeva & Buratowski, 2006
yBD154	*MATα; ura3-1; trp1-1; rna14-1; nrd1Δ::KANMX; [pRS424nrd1-2 (nrd1-2, TRP1, 2 μ ori)]*	*rna14-1 nrd1-2*	Vasiljeva & Buratowski, 2006
yBD155	*MATα; ura3-1; trp1-1; rna14-1; nrd1Δ::KANMX; [pRS314NRD1Δ39-169 (nrd1ΔCID(39-169), TRP1, CEN)]*	*rna14-1 nrd1ΔCID*	Vasiljeva & Buratowski, 2006
yBD171	*MATa ura3-52 leu2-3,112 trp1-1 his3-11,15 nrd1::HIS3 lys2Δ2 ade2-1 met2Δ1 can1-100, (pRS 316 NRD1(NRD1, URA3,CEN)) rrp6::TRP1*	*rrp6-Δ*	This Study[¥¥]
yBD183	*MATa; ura3-52; leu2-3,112; trp1-1; his3-11,15; nrd1Δ::HIS3; lys2Δ2; ade2-1; met2Δ1, can1-100 [pRS316NRD1 (NRD1, URA3, CEN)]; cbc1Δ::TRP1*	*cbc1-Δ*	This Study[¥]
yBD177	*MATa ura3-52 leu2-3,112 trp1-1 his3-11,15 nrd1::HIS3 lys2Δ2 ade2-1 met2Δ1 can1-100, (pRS 424nrd1-1(nrd1-1, TRP1, 2μ ori))*	*nrd1-1*	Vasiljeva & Buratowski, 2006
yBD159	*MATa ura3-52 leu2-3,112 trp1-1 his3-11,15 nrd1::HIS3 lys2Δ2 ade2-1 met2Δ1 can1-100, (pRS 424nrd1-2(nrd1-2, TRP1, 2μ ori))*	*nrd1-2*	Vasiljeva & Buratowski, 2006
yBD149	*MATa; ura3-52; leu2-3,112; trp1-1; his3-11,15;nrd1Δ::HIS3; lys2Δ2; ade2-1; met2Δ1, can1-100; [pRS314NRD1Δ39-169 (nrd1ΔCID(39-169), TRP1,CEN)]*	*nrd1ΔCID*	Vasiljeva & Buratowski, 2006
yBD316	*MATa; ura3-52; leu2-3,112; trp1-1; his3-11,15; nrd1Δ::HIS3; lys2Δ2; ade2-1; met2Δ1, can1-100 [pRS316NRD1 (NRD1, URA3, CEN)] pBD250(pRSII315 lys2-187)*	*lys2-187*	This Study[¥]
yBD317	*MATa ura3-52 leu2-3,112 trp1-1 his3-11,15 nrd1::HIS3 lys2Δ2 ade2-1 met2Δ1 can1-100, (pRS 316 NRD1(NRD1, URA3,CEN)) rrp6::TRP1 pBD250(pRSII315 lys2-187)*	*lys2-187 rrp6-Δ*	This Study[¥]
yBD318	*MATa; ura3-52; leu2-3,112; trp1-1; his3-11,15; nrd1Δ::HIS3; lys2Δ2; ade2-1; met2Δ1, can1-100 [pRS316NRD1 (NRD1, URA3, CEN)]; cbc1Δ::TRP1 pBD250(pRSII315 lys2-187)*	*lys2-187 cbc1-Δ*	This Study[¥]

yBD319	*MATa ura3-52 leu2-3,112 trp1-1 his3-11,15 nrd1::HIS3 lys2Δ2 ade2-1 met2Δ1 can1-100, (pRS 424nrd1-1(nrd1-1, TRP1, 2μ ori)) pBD250(pRSII315 lys2-187)*	*lys2-187 nrd1-1*	This Study[¥]
yBD320	*MATa; ura3-52; leu2-3,112; trp1-1; his3-11,15; nrd1Δ::HIS3; lys2Δ2; ade2-1; met2Δ1, can1-100; [pRS424nrd1-2 (nrd1-2, TRP1, 2 μ ori)] pBD250(pRSII315 lys2-187)*	*lys2-187 nrd1-2*	This Study[¥]
yBD384	*MATa; ura3-52; leu2-3,112; trp1-1; his3-11,15;nrd1Δ::HIS3; lys2Δ2; ade2-1; met2Δ1, can1-100; [pRS314NRD1Δ39-169 (nrd1ΔCID(39-169), TRP1,CEN)]pBD250(pRSII315+lys2-187)*	*lys2-187 nrd1ΔCID*	This Study[¥]
yBD277	*MATa; ura3-52; leu2-3,112; trp1-1; his3-11,15; nrd1Δ::HIS3; lys2Δ2; ade2-1; met2Δ1, can1-100 [pRS316NRD1 (NRD1, URA3, CEN)]nup116::LEU2*	*nup116-Δ*	This Study[¥]
yBD278	*MATa ura3-52 leu2-3,112 trp1-1 his3-11,15 nrd1::HIS3 lys2Δ2 ade2-1 met2Δ1 can1-100, (pRS 316 NRD1(NRD1, URA3,CEN)) rrp6::TRP1 nup116::LEU2*	*nup116-Δ rrp6-Δ*	This Study[¥]
yBD279	*MATa; ura3-52; leu2-3,112; trp1-1; his3-11,15; nrd1Δ::HIS3; lys2Δ2; ade2-1; met2Δ1, can1-100 [pRS316NRD1 (NRD1, URA3, CEN)]; cbc1Δ::TRP1 nup116::LEU2*	*nup116-Δ cbc1-Δ*	This Study[¥]
yBD280	*MATa; ura3-52; leu2-3,112; trp1-1; his3-11,15; nrd1Δ::HIS3; lys2Δ2; ade2-1; met2Δ1, can1-100; [pRS424nrd1-2 (nrd1-2, TRP1, 2 μ ori)] nup116::LEU2*	*nrd1-2 nup116-Δ*	This Study[¥]
yBD215	*MatX;ura3-52;leu2-3,112;pep4-3;SEN1*	*SEN1+*	Ursic *et al.*, 1997
yBD217	*MatX;ura3-52;leu2-3,112;pep4-3;SEN1;rrp6Δ::KanMx*	*rrp6-Δ*	Ursic *et al.*, 1997
yBD219	*MATx;ura3-52;leu2-3,112;pep4-3;SEN1;cbc1::hisG URA3*	*cbc1-Δ*	This Study[¥]
yBD216	*MatX;ura3-52;leu2-3,112;pep4-3;sen1-1*	*sen1-1*	Ursic *et al.*, 1997
yBD91	*MATa ade2-1 can1-100 his3-11,15 leu2-3,112 trp1-1 ura3-1*	*NAB3+*	This Study[¥]
yBD261	*MATa ade2-1 can1-100 his3-11,15 leu2-3,112 trp1-1 ura3-1; rrp6::URA3*	*rrp6-Δ*	This Study[¥]
yBD262	*MATa ade2-1 can1-100 his3-11,15 leu2-3,112 trp1-1 ura3-1; cbc1::hisG URA3 hisG*	*cbc1-Δ*	This Study[¥]
yBD250	*MATa ade2 can1-100 his3-11,15 leu2-3,-112 trp1-1 ura3-1 nab3-10*	*nab3-10*	Conrad *et al*., 2000
yBD414	*Matα leu2-3,112 his3-11,15 trp1-1 ade2-1 can1-100 ura3-1*	*PCF11+*	Medler *et al.*, 2011
yBD408	*MATa leu2-3,112 his3-11,15 ade2-1 ura3-1 trp1-1rrp6::URA3*	*rrp6-Δ*	This Study[¥]
yBD409	*MATa leu2-3,112 his3-11,15 ade2-1 ura3-1 trp1-1cbc1::URA3*	*cbc1-Δ*	This Study[¥]
yBD415	*Mata ura3-1trp1Δ ade2-1 leu2-3,112 his3-11,15 pcf11-Δ::TRP1/ pEL36 pcf11-2*	*pcf11-2*	Medler *et al.*, 2011
yBD 259	*MATa; ura3-52; leu2-3,112; trp1-1; his3-11,15; nrd1Δ::HIS3; lys2Δ2; ade2-1; met2Δ1, can1-100; [pRS424nrd1-2 (nrd1-2, TRP1, 2 μ ori)];rrp6::URA3*	*rrp6-Δnrd1-2*	*This Study*[¥]
yBD 260	*MATa; ura3-52; leu2-3,112; trp1-1; his3-11,15; nrd1Δ::HIS3; lys2Δ2; ade2-1; met2Δ1, can1-100; [pRS424nrd1-2 (nrd1-2, TRP1, 2 μ ori)];cbc1::hisG URA3 hisG (Blaster)*	*cbc1-Δnrd1-2*	*This Study*[¥]

[¥]Constructed in the laboratory during the period of work

Table EV2: List of Plasmids used in this study

Plasmid No.	Description	Use	Reference
pBD237	A 2522bp *LEU2* fragment (BsrGI /SpeI digest) was cloned into BsrGI/NheI site of *HPR1* cloned in pJET. Digest with NsiI and transform.	HPR1 Disruptor	This work[¥]
pBD 251	A pRS II 316 containing full-length *NRD1* gene (from mother stain yBD148) was transformed into DH5α	*NRD1* cloned in pRS II 316	This work[¥]
pBD276	A pRS II 424 containing *nrd1-1* gene fragment (from mother stain yBD177) was transformed into DH5α	*nrd1-1* cloned in pRS II 424	This work[¥]
pBD 257	A pRS II 424 containing *nrd1-2* gene fragment (from mother stain yBD159) was transformed into DH5α	*nrd1-2* cloned in pRS II 424	This work[¥]
pBD275	A pRS II 314 containing *nrd1ΔCID* gene fragment (from mother stain yBD149) was transformed into DH5α	*nrd1ΔCID* cloned in pRS II 424	This work[¥]
pBD 28	A 4.5 kb. *CBC1* gene cloned in SalI and HindIII sites of pUC19 containing the complete ORF and 5′ and 3′ UTR and is functional. BamHI site of this pUC19 is destroyed.	*CBC1* cloned in pUC19	Das et al. (2000)
pBD160	A 1448 bp (SspI/ BglII) *TRP1* fragment from pBD 135 was cloned at AvrII/BglII site of pBD 28.	*CBC1*-TRP1 Disruptor	This work[¥]
pBD162	A 5kb *LYS2* fragment from pBD 58 cloned into pRSII316/pBD121. It is a XbaI+HindIII fragment	*LYS2* cloned in pRS II 316	This work[¥]
pBD 249	A PfiMI/BamHI fragment of *lys2-187* (OBD 481+496) cloned at PfiMI/BamHI site of pBD 162	*lys2-187* cloned in pBD162	This work[¥]
pBD250	A 4.9kb XbaI/SalI/BglI *lys2-187* fragment cloned into theXbaI/SalI site of pBD118 Plasmid	*lys2-187* cloned in pRS II 315	
pBD 49	URA3 disruptor in pBSKS of *NUP116* gene from Susan Wente. Digest with EcoRI and transform.	*NUP116* Disruptor	Wente et al. (1992)
pBD 45	A 1.4 kb fragment carrying 1.1 kb *URA3* gene flanked by 5′ and 3′ flanking sequence of *RRP6* gene in pUC19.	*RRP6* Disruptor	(Briggs et al.,1998)
pBD42	A 4.1kb fragment containing the *CBC1* (from pBD 32) fragment is cloned in pCR 2.1 vector containing 5′ and 3′ part of *CBC1* ORF and Blaster.	*CBC1*-Blaster Disruptor	(Das et al., 2000)
pBD236	A 1.5 Kb *LEU2* fragment (PfiMI digest) cloned into StuI/NdeI site of pBD49	*NUP116* Disruptor	This work[¥]

[¥]Constructed in the laboratory during the period of work

Table EV3: List of Oligonucleotides used in this study

Oligo No.	Name	Sequence	Gene to Amplify	Reference
OBD5	BD-RRP6-D-S1	5′- AGAATTTAGACAGGGG-3′	*RRP6*$^{+}$	Briggs *et al.*, 1998
OBD6	BD-RRP6-D-AS1	5′-CAT CGTCTCTTCTTGC-3′		
OBD19	CBC1-BLASTER 5′ JUNCTION-S1	5′ CGAATGTAGTCCATCCTCCGAATC-3′	*CBC1* Blaster	Das *et al.* 2000
OBD20	CBC1-BLASTER 5′ JUNCTION-AS1	5′ TGTGCTCCTTCCTTCGTTCTTCCT-3′		
OBD24	CBC1-BLASTER 3′ JUNCTION-AS2	5′CATACCCAACTTTGACTACCTTGC-3′	*CBC1* Blaster	Das *et al.* 2000
OBD25	CBC1-BLASTER 3′ JUNCTION-S2	5′TGATGATGACATTCCGGGTCTGGT-3′		
OBD41	AM-NUP116-D-S5	5′- ACTCATGCCCATCTCGTCCCT -3	*NUP116*	Maity *et al.*, 2016
OBD42	AM-NUP116-D-AS5	5′-ACCTTGGCATTCGCACCGCT -3		
OBD146	AM-ACT1-S1	5’-TGACGACGCTCCTCGTGCTG 3’	*ACT1*	Maity *et al.*, 2016
OBD177	AM-ACT1-AS3	5'- GGCAACTCTCAATTCGT -3'		
OBD168	AM-SCR1-S2	5′-TTGTGGCAACCGTCTTTCCT- 3′	*SCR1*	Das *et al.*, 2014
OBD169	AM-SCR1-AS2	5′- CCGAAGCGATCAACTTGCAC 3’		
OBD184	AM-CYC1-RT-S1	5′-AAAGGGTGGCCCACATAAGG- 3′	*CYC1*	This work[Y]
OBD185	AM-CYC1-RT-AS1	5′- CTTCAACCCACCAAAGGCCA-3′		
OBD186	AM-CYC1-RT	5'-AATTCAAGGCCGGTTCTGCT-3'		
OBD212	PS-CBC1-DS2	5'-TATACGCGTTTGGGGCTACA-3'	*CBC1*	This work[Y]
OBD213	PS-CBC1-DAS2	5'-GCATTACTTTCCCGAACCGC-3'		
OBD214	PS-RRP6-S3	5'-TGAGGCAAAGGACGCACATA-3'	*RRP6*	This work[Y]
OBD215	PS-RRP6-AS3	5'-TTCCTGACACCGTCCATTCG-3'		
OBD246	AM-RT-ACT1-EIJ-S2	5′-AGAAGAATTGCACGGTCCCA- 3	Intronic Region of *ACT1*	Maity *et al.*, 2016
OBD247	AM-RT-ACT1-EIJ-AS2	5′AGCAACAAAAAGAATGAAGCAATCG - 3′		
OBD268	US-ACT1-RT-S1	5′-GCCGAAAGAATGCAAAAGGA-3′	*ACT1*	Das *et al.*, 2014
OBD269	US-ACT1-RT-AS1	5′-TCTGGAGGAGCAATGATCTTGA-3		
OBD270	US-ACT1-RT-S2	5'- TGGATTCCGGTGATGGTGTT-3'	*ACT1*	Maity *et al.*, 2016
OBD271	US-ACT1-RT-AS2	5'- TCAAAATGGCGTGAGGTAGAGA-3'		
OBD280	AM-RT-CYH2-INT-S1	5′-GTGCAACCAATATGTCGTGTGT-3′	*CYH2*	
OBD281	AM-RT-CYH2-INT-AS1	5′- GCGCTCTCTACAACCATTTGA -3′		
OBD341	AM-RT-18S-S2	5'-GATCGGGTGGTGTTTTTTTAATG-3'	*18S*	This work[Y]
OBD342	AM-RT-18S-AS2	5'-CTCCCCCCAGAACCCAAA-3'		
OBD415	PS-HPR1-S1	5’-CCGTGCGATTTCAAGACTGC-3’	*HPR1*$^{+}$	This work[Y]
OBD416	PS-HPR1-AS1	5’- AGGATCTCTGTGGTACGCTA-3’		
OBD445	PS-HPR1-F	5'- ACTGCTCATTTCGCACGATG-3'	*HPR1*$^{+}$	This work[Y]
OBD446	PS-HPR1-R	5'-AGCAAAGGGACTTCTAAGGACG-3'		
OBD551	PS-NRD1-F	5'-TCCTCGTTAGCATGACTCCC-3'	*NRD1*$^{+}$	This work[Y]
OBD552	PS-NRD1-R	5'-AATATGCCGGAAACGTCCA-3'		
OBD588	CYC1-R(START)	5'-ACGGTGTGGCATTGTAGACATC-3'	*CYC1*	This work[Y]
OBD589	CYC1-R(MID)	5'-TACGAATACCCTTCAGCTTGACC-3'		
OBD459	AM-CYC1-EX1_S1	5'- ATGGCCTTTGGTGGGTTGAA-3'	*CYC1*	This work
OBD460	AM-CYC1-EX1_AS1	5'-TCCTTTTCGGTTAGAGCGGA-3'		

OBD 467	CYC1-EX2-S2	5'-TGG CTT ACG ATC ACG ATG TCA-3'	*CYC1* (*C2*)	Maity et al., 2016
OBD 468	CYC1-EX2-AS2	5'-TGCTCTTTCATGCATCCTGAA 3'		
OBD469	LYS2-EX2-S2	5' CGGATTGGCTGAGTCACCTT 3'	*LYS2* (*L2*)	Maity et al., 2016
OBD594	PS_IMP3_STARTF	5'-ATGGAAGCAGGACCAAGGC-3'	*IMP3*	This work[Y]
OBD595	PS_IMP3_STARTR	5'-ATGGAAGCAGGACCAAGGC-3'		
OBD596	PS_IMP3_MIDF	5'CATTATTACCTCCCACTGATCCATT-3'		
OBD597	PS_IMP3_MIDR	5'CCCATAGCGTATAGCTTGTCCAGTA-3'		
OBD598	PS_IMP3_END F	5'-GCGTGGGTCCAAATTTGATC-3'		
OBD599	PS_IMP3_END R	5'CACCCAAGTAACGTAGTCCTCCATA-3'		
OBD586	PS-NCW2- STARTF	5'-CTAGCCGCTGCTCAAAAAGAC-3'	*NCW2*	This work[Y]
OBD587	PS-NCW2- STARTR	5'-CCTTTTGTGAGCTATCTTCAGAGTTCT-3		
OBD278	US-NCW2-RT-S6	5'-GCACAACTTCAACTGCCTCTGT-3'		
OBD279	US-NCW2-RT-AS6	5’-GGATGCGGAGTTGGTGATTC-3’		
OBD276	US-NCW2-RT-S5	5′-AGCGTCCGTAATGTCCAATTCT-3′		
OBD277	US-NCW2-RT-AS5	5′-CCCGCACCATAAGCTATGTGA-3′		
OBD274	US-SKS1-RT- S1	5’- CCTACTGGATCGCAATGACAAC-3’	*SKS1*	This work[Y]
OBD275	US-SKS1-RT- AS1	5’- CGCACACATTTGGAGCTAGATATT-3’		
OBD311	PS-SKS1-RT-1202bp-F	5-'TACAAAACCAGGAACAAGCACAA-3'		
OBD312	PS-SKS1-RT-1242bp-F	5-'TCACTCTCCGGTTCAGCATCT-3'		

Legends to the Extended View Figures

Figure EV1. Steady-state levels of diverse aberrant mRNPs generated in transcription-elongation-(*hpr1*-Δ) (A), splice-(*prp2-1*) (B) and 3′-end processing-(*rna14-1*) defective (C) yeast strains at 25°C. Scatter plot revealing the relative abundance at 25°C of (A) transcription assembly-defective *ACT1* and *CYC1* mRNAs in the isogenic *hpr1*-Δ strains, (B) of intron-containing precursor pre-*ACT1* and pre-*CYH2* transcripts in the isogenic *prp2-1* strains, and (C) the 3′-extended transcripts of *LYS2* and *CYC1* genes in the isogenic *rna14-1* strains. For (A), the mean normalized level of each target mRNAs estimated in the $HPR1^+$ sample was set to 1. For (B) and (C) the normalized value of each pre-mRNA signal from *prp2-1* and *rna14-1* samples was set to 1 The RNA extraction and steady-state levels of the specific mRNAs were determined exactly as described in the legend of Figure 3

Figure EV2. (A-B) Schematic presentation of the approximate locations of the primer-sets and corresponding amplicons used for qRT-PCR analyses for the intron-containing pre-*ACT1*, pre-*CYH2* messages in *prp2-1* isogenic strain series (A), and aberrant 3′-end extended read-through *LYS2* and *CYC1* mRNAs in *rna14-1* isogenic strain series (B). Note that the length and location are not up to the scale. **(C) Relative steady-state levels of normal *CYC1* mRNA at 25°C in the indicated isogenic yeast strains.** The normalized value of the *CYC1* transcript from the $LYS2^+$ sample was set to 1. The RNA extraction and steady-state levels of the specific mRNAs were determined exactly as described in the legend of Figure 3**. (D-E) Scatter plot revealing the relative steady-state levels of *ACT1* (D) and *CYC1* at 25°C (E) in the indicated isogenic *nup116*-Δ mutant strains.** The normalized value of these transcripts from the *nup116*-Δ sample was set to 1. The RNA extraction and steady-state levels of the specific mRNAs were determined exactly as described in the legend of Figure 3. **(F) Growth profile of $LYS2^+$ and the isogenic *lys2-187* mutant strains on SC-Lys medium at 25°C.** A series of progressively diluted ($1/10^{th}$) suspension from the stock (concentration 10^5/cells per ml) of each strain were made, followed by spotting (10 μl) on lysine omission medium (SC-Lys). The plates were incubated at 25°C for either 3-4 days, and the image was captured.

Figure EV3. Nrd1p acts together with the core nuclear exosome, and the CTEXT complex to target the export defective special mRNAs and its co-transcriptional recruitment is crucial for the nuclear decay of these transcripts. (A-C) Scatter plot revealing the relative steady-state levels of two

export-inefficient special, *NCW2* (A) and *SKS1* mRNAs (B), and normal *CYC1* mRNA (C) at 25°C in an isogenic wild type, *rrp6*-Δ, *cbc1*-Δ, *nrd1-2*, *rrp6*-Δ *nrd1-2*, and *rrp6*-Δ *nrd1-2* strains. The normalized value of each specific mRNAs from the wild-type sample was set to 1. The RNA extraction and steady-state level of the specific mRNAs were determined as described in the legend of Figure 3. (D-F) Nrd1p occupancy profiles of the transcription-assembly-defective *ACT1* (D) and *CYC1* (E) in an *hpr1*-Δ strain at 25°C and 37°C, normal *CYC1* and special *NCW2* mRNAs (F) in a wild-type yeast strain at 25°C. All immunoprecipitations using specific Nrd1p antibody followed by the recovery of the precipitated DNA and qPCR analyses were performed exactly as described in materials and methods and the legend of Figure 4. The primer sets specific for the middle region corresponding to the ORF of each target mRNA were used for the qPCR analyses to generate these scatter plots. (G) Western blot showing the specificity of the anti-Nrd1p antibody and expression level of Nrd1p in the isogenic yeast strain harboring $NRD1^{+}$ and $nrd1\Delta^{CID}$ allele. Each lane contained an equal amount of quantified protein extracts from the indicated strains. A 70 kDa band in the extract from *NRD1+* strain and 55 kDa band in the extract from $nrd1\Delta^{CID}$ was detected with no non-specific band.

Figure EV4. (A-C) Scatter plot revealing the relative steady-state levels of normal *CYC1* (negative control) at 25°C in the indicated *nrd1* (A), *nab3* (B), and *sen1* isogenic yeast strain series. Normalized values of the transcript in the wild-type samples were set to 1. The RNA extraction and steady-state levels of the specific mRNAs were determined exactly as described in the legend of Figure 3. **(D-I) Scatter plot revealing the relative steady-state levels of export-inefficient nucleus-arrested special *IMP3* (D-E) *NCW2* (F-G) and *SKS1* (H-I) mRNAs at 25°C in the indicated *nab3* (D, F, H) and *sen1* (E, G, I) isogenic yeast strain series.** Normalized values of all the transcripts in the wild-type samples were set to 1. The RNA extraction and steady-state levels of the specific mRNAs were determined exactly as described in the legend of Figure 3.

Figure EV5. Co-transcriptional recruitment of full-length Nrd1p and Nrd1p lacking the *CID* domain on (A) transcription assembly-defective, (B) splice-defective and (C) 3′-extended aberrant messages, and (D) export-defective special messages. Occupancy profile of full-length Nrd1p and Nrd1p lacking its *CID* domain of the (A) transcription-assembly-defective *ACT1* and *CYC1* mRNAs at 37°C in isogenic *hpr1*-Δ and *hpr1*-Δ *nrd1ΔCID* strains, (B) splice-defective intron-containing pre-*ACT1* and pre-*CYH2* at 37ºC in isogeneic *prp2-1* and *prp2-1 nrd1ΔCID* strains (C) 3′-extended read-

through *CYC1* and *LYS2* transcripts at 37ºC in *rna14-1* and *rna14-1 nrd1ΔCID* strains and (D) nucleus-arrested special messages *NCW2* and *SKS1* at 25ºC in wild-type (*NRD1*$^{+}$) and *nrd1ΔCID* strains. All immunoprecipitation using specific Nrd1p antibody followed by the recovery of the precipitated DNA and qPCR analyses was performed exactly as described in materials and methods and the legend of Figure 4D-F. The primer sets specific for the 5′-end and 3′-end corresponding to the ORF of each target mRNA were used for the qPCR analyses to generate these scatter plots.

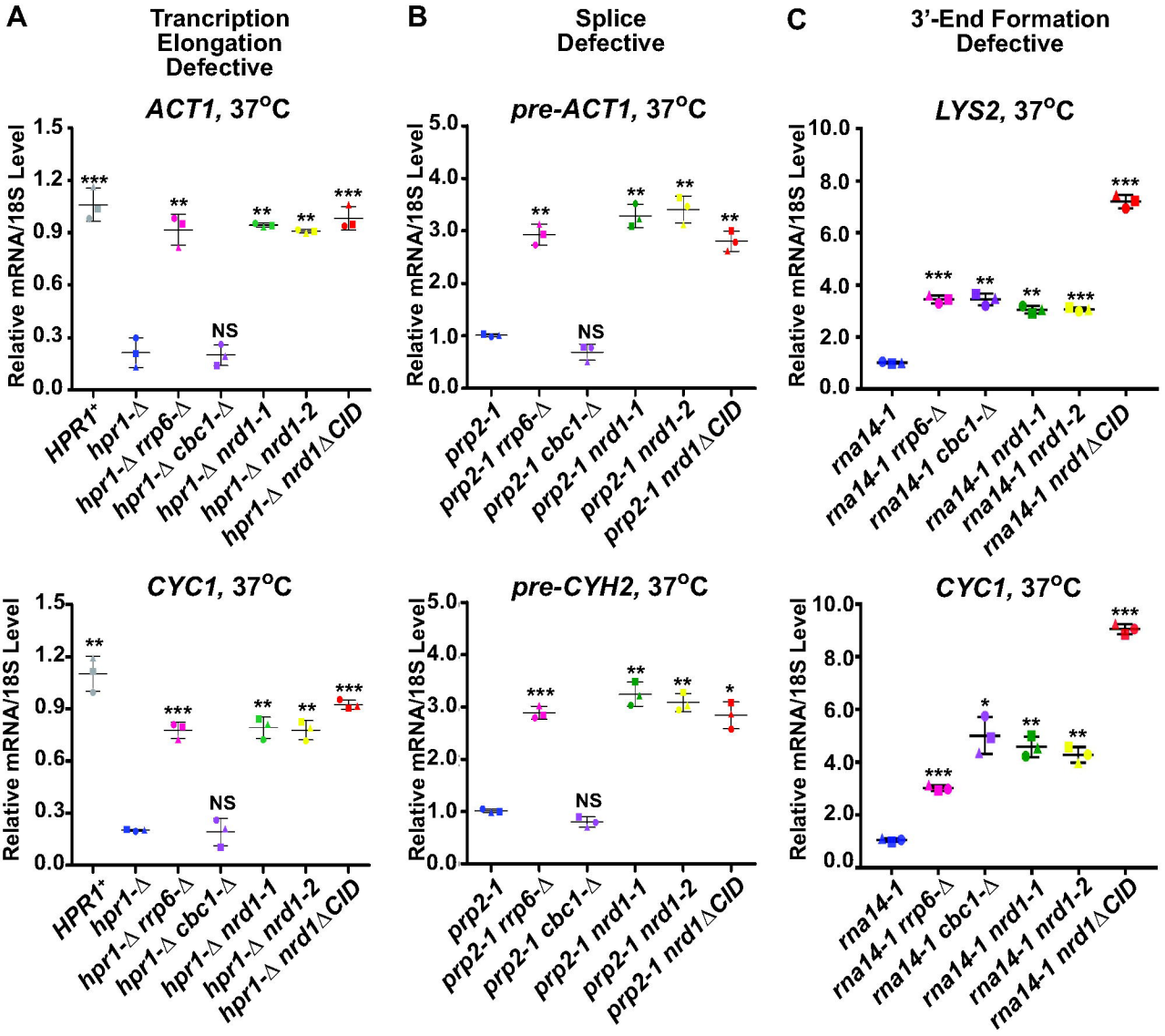

EMBOR-2020-51007V1_Fig1.eps
Singh et al., 2020

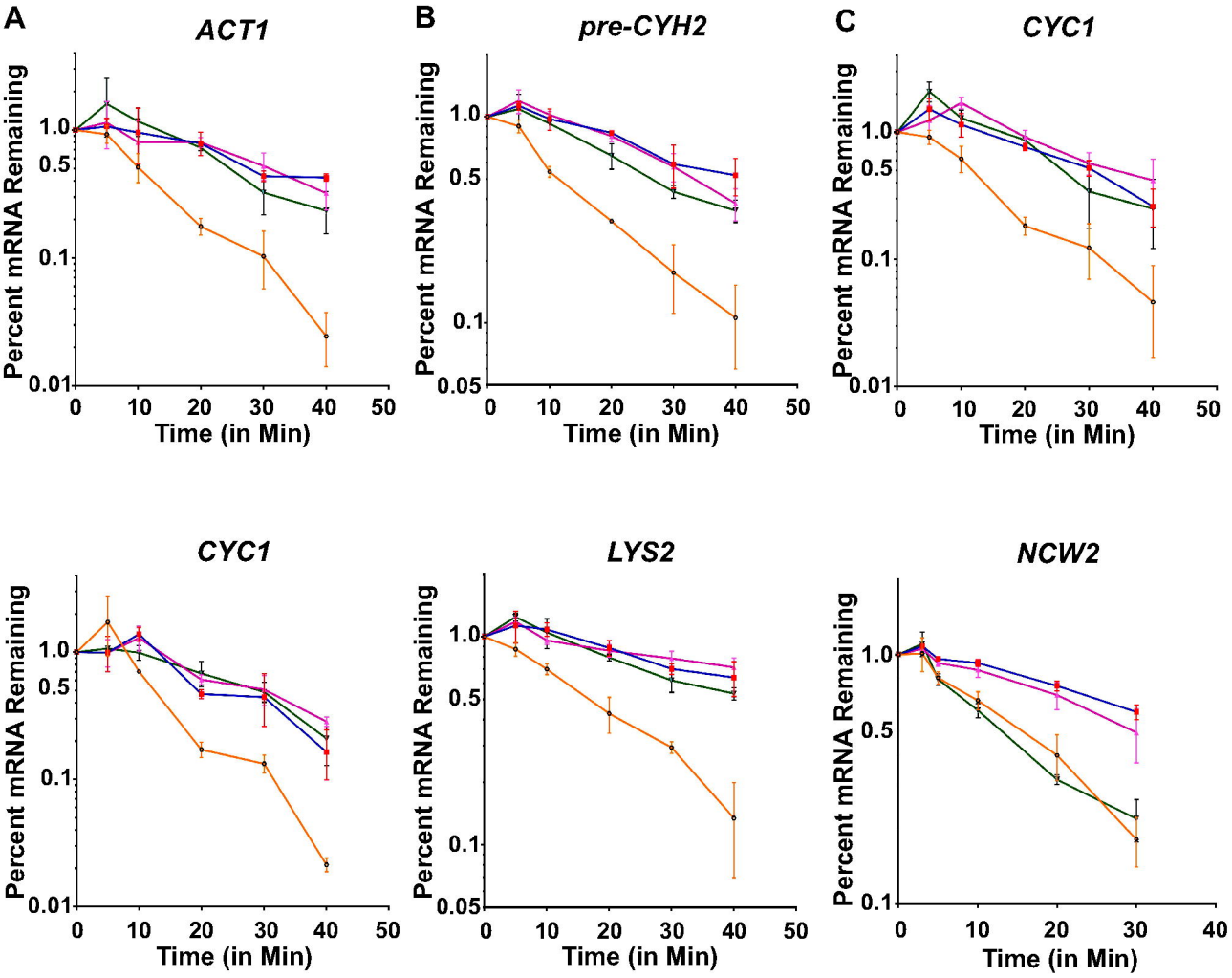
A
ACT1
B
pre-CYH2
C
CYC1
CYC1
LYS2
NCW2
Percent mRNA Remaining
Time (in Min)
1.0
0.5
0.1
0.01
0.05
0
10
20
30
40
50

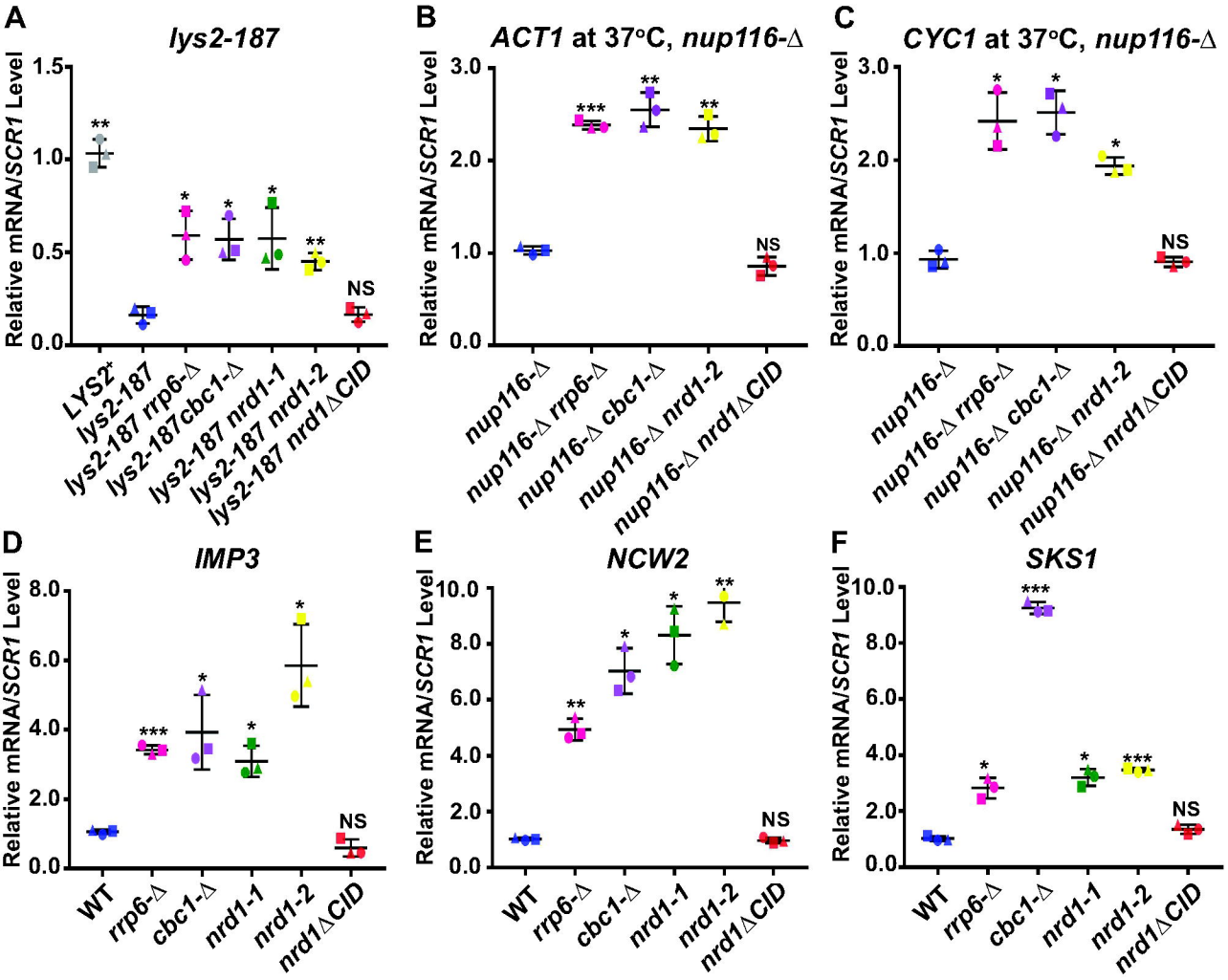
A
lys2-187
Relative mRNA/SCR1 Level
1.5
1.0
0.5
0.0
**
*
*
*
**
NS
LYS2+
lys2-187
lys2-187 rrp6-Δ
lys2-187cbc1-Δ
lys2-187 nrd1-1
lys2-187 nrd1-2
lys2-187 nrd1ΔCID
B
ACT1 at 37°C, nup116-Δ
Relative mRNA/SCR1 Level
3.0
2.0
1.0
0.0
***
**
**
NS
nup116-Δ
nup116-Δ rrp6-Δ
nup116-Δ cbc1-Δ
nup116-Δ nrd1-2
nup116-Δ nrd1ΔCID
C
CYC1 at 37°C, nup116-Δ
Relative mRNA/SCR1 Level
3.0
2.0
1.0
0.0
*
*
*
NS
nup116-Δ
nup116-Δ rrp6-Δ
nup116-Δ cbc1-Δ
nup116-Δ nrd1-2
nup116-Δ nrd1ΔCID
D
IMP3
Relative mRNA/SCR1 Level
8.0
6.0
4.0
2.0
0.0
***
*
*
*
NS
WT
rrp6-Δ
cbc1-Δ
nrd1-1
nrd1-2
nrd1ΔCID
E
NCW2
Relative mRNA/SCR1 Level
10.0
8.0
6.0
4.0
2.0
0.0
**
*
*
**
NS
WT
rrp6-Δ
cbc1-Δ
nrd1-1
nrd1-2
nrd1ΔCID
F
SKS1
Relative mRNA/SCR1 Level
10.0
8.0
6.0
4.0
2.0
0.0
***
*
*
***
NS
WT
rrp6-Δ
cbc1-Δ
nrd1-1
nrd1-2
nrd1ΔCID

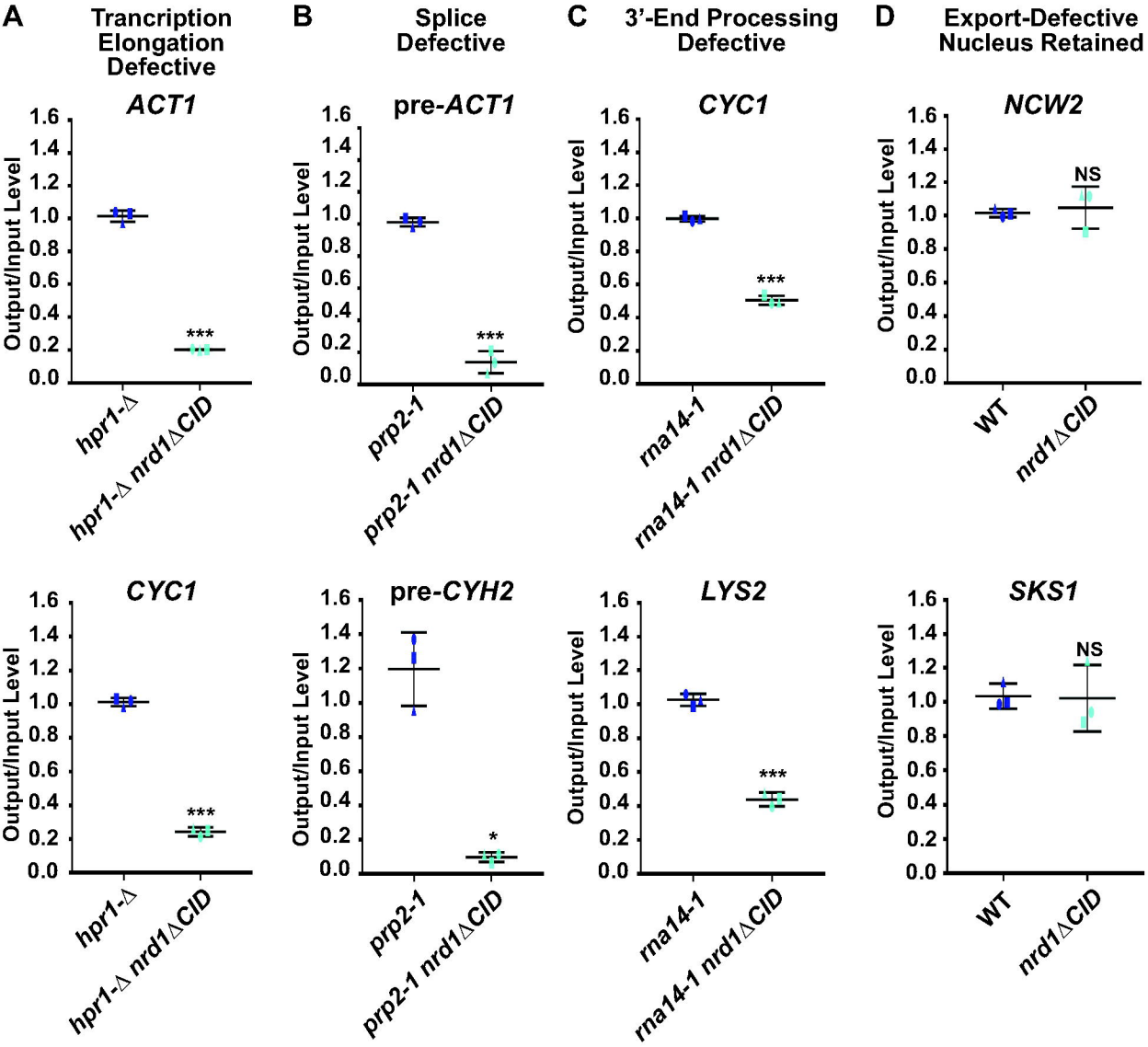

EMBOR-2020-51007V1_Fig 4.eps
Singh et al., 2020

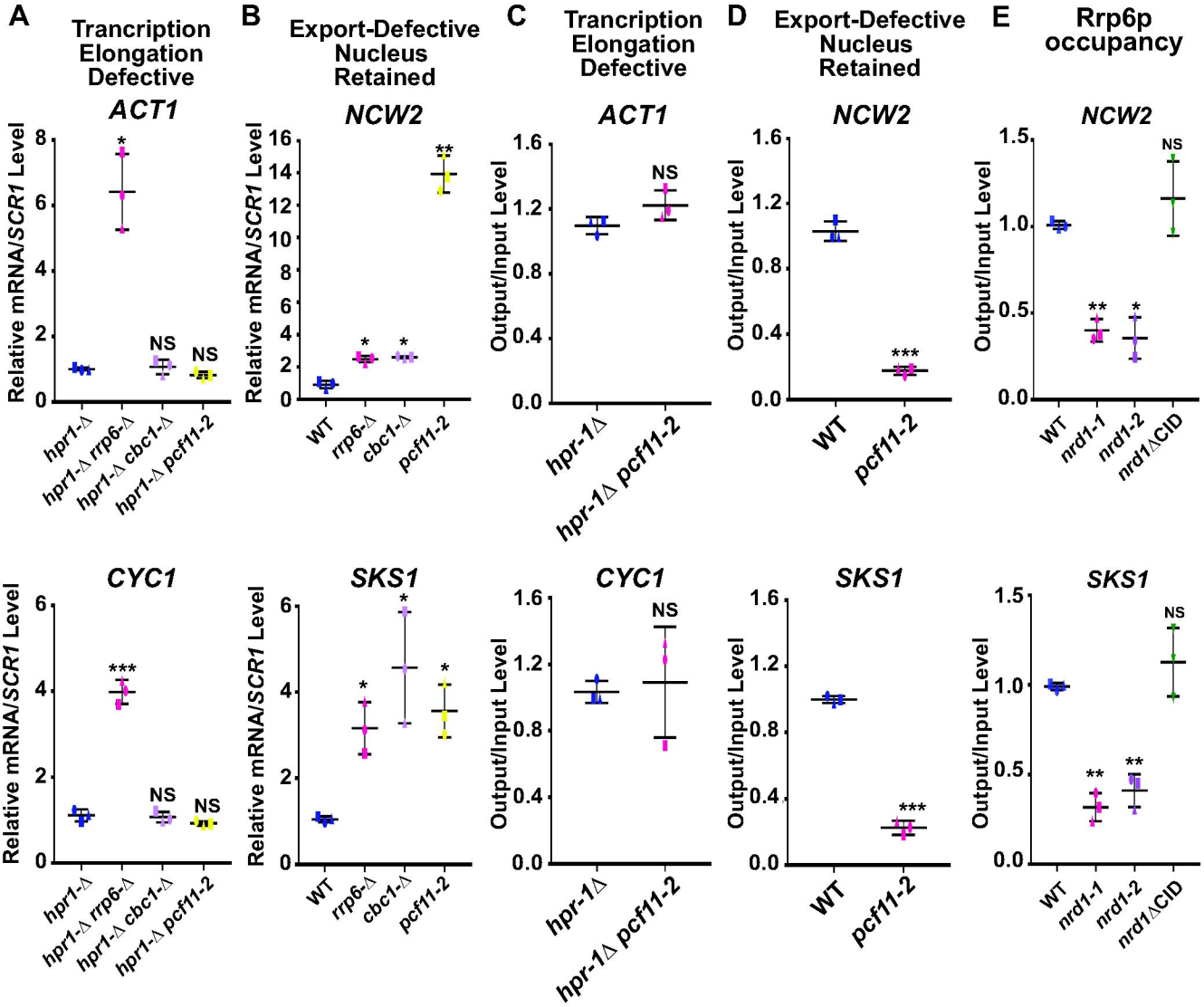

EMBOR-2020-51007V1_Fig 5.eps
Singh et al., 2020